

Impact de la variabilité atmosphérique interannuelle et du changement climatique sur la formation et l'exportation d'eau dense sur le plateau du golfe du Lion

Sommaire

9.1	Introduction	147
9.2	Tools and methods	149
9.2.1	Modeling strategy	149
9.2.2	The numerical eddy-resolving regional oceanic model	150
9.2.3	Dense water criteria	151
9.3	Impact of interannual variability on the dense water formation and transport under present-day climate conditions	153
9.3.1	Formation of dense water over the shelf	155
9.3.2	Elimination of dense water	155
9.3.3	Export of dense water	157
9.3.4	Comparison with available data	158
9.4	Impact of climate change	160
9.5	Extrapolation to the whole present and future periods	164
9.6	Uncertainties	168
9.6.1	Sensitivity test to the dense water criteria	168
9.6.2	Sensitivity to the parameters of the regional oceanic model	169
9.6.3	Sensitivity to the water flux	171
9.6.4	Sensitivity test to the Atmospheric Regional Climate Model (ARCM)	172
9.7	Conclusion	181

Dans les chapitres 7 et 8, nous avons étudié la formation d'eau dense au large, qui a lieu pendant la convection océanique profonde, puis le devenir de cette eau dense, en Méditerranée nord-occidentale. Nous nous intéressons ici à la formation et au devenir de l'eau dense sur le plateau continental. Cette étude a fait l'objet d'un article en révision au *Continental Shelf Research* [Herrmann *et al.*, 2008a]. Nous présentons dans ce chapitre un résumé en français des résultats et conclusions obtenus, puis l'article proprement dit.

RESUME DE L'ARTICLE

Dans certaines régions côtières des océans mondiaux (voir paragraphe 2.2.2), les conditions atmosphériques hivernales peuvent en effet être à l'origine de la formation de masses d'eaux particulièrement denses [Ivanov *et al.*, 2004; Durrieu de Madron *et al.*, 2005]. Ces masses d'eau dense coulent par gravité le long du talus continental, entraînant avec elles au fond des océans de grandes quantités de sédiments et de matière organique. Ce processus de *cascading* d'eau dense contribue ainsi au stockage du carbone dans l'océan profond.

Plusieurs épisodes de *cascading* d'eau dense ont été observés dans les canyons qui incisent le talus continental du golfe du Lion [Durrieu de Madron *et al.*, 2005; Béthoux *et al.*, 2002a; Canals *et al.*, 2007], une zone d'accès relativement aisé pour les campagnes océanographiques et où les apports continentaux et la productivité biologique sont élevés, dus notamment à la présence du Rhône. L'eau dense cascadant le long des canyons vers l'océan profond entraîne avec elle des masses importantes de sédiments et de matière organique, influençant alors le fonctionnement des écosystèmes marins profonds et les caractéristiques géologiques des canyons [Monaco *et al.*, 1990; Béthoux *et al.*, 2002a; Palanques *et al.*, 2006; Gaudin *et al.*, 2006; Heussner *et al.*, 2006; Canals *et al.*, 2007]. D'après Heussner *et al.* [2006], le *cascading* serait majoritairement responsable de l'exportation de matière particulaire vers les zones profondes du golfe du Lion, et expliquerait sa variabilité interannuelle. Ces auteurs soulignent cependant que les données disponibles n'ont pas permis d'établir de relation causale claire.

Quelques évaluations chiffrées des volumes d'eau et de matière organique transportés vers le fond ont été effectuées pour les hivers 1998-99 et 2004-05 ainsi que pour la période 1993-2001 par Durrieu de Madron *et al.* [2005], Béthoux *et al.* [2002a], Heussner *et al.* [2006], Palanques *et al.* [2006] et Canals *et al.* [2007]. Une première étude expérimentale de la variabilité spatiale et temporelle des transferts de matière entre le plateau et le large a été réalisée par Heussner *et al.* [2006]. En outre, des études numériques ont été menées par Dufau-Julliand *et al.* [2004] et Ulses *et al.* [2008] pour les hivers 1998-99 et 2004-05, montrant que le modèle utilisé, SYMPHONIE, était capable de reproduire correctement les caractéristiques principales d'épisodes de *cascading* réel. Un des objectifs de l'article présenté dans ce chapitre est d'utiliser ce modèle afin de fournir des estimations des volumes annuels d'eau formée et transportée vers le large et le fond, et d'évaluer leur variabilité interannuelle, ce qui permettrait de compléter le travail de Heussner *et al.* [2006].

Somot *et al.* [2006] ont montré que le changement climatique pourrait affaiblir notablement la convection profonde au large du golfe du Lion ainsi que la formation d'eau dense associée d'ici la fin du XXI^e siècle. Le phénomène de *cascading* étant largement conditionné par les conditions atmosphériques, on peut s'attendre à ce

qu'il soit également affecté par le changement climatique. Le second objectif de l'article qui suit est de proposer une première quantification des éventuels effets du changement climatique sur ce processus.

Pour cela, nous réalisons une étude numérique tridimensionnelle afin d'étudier les effets de la variabilité atmosphérique interannuelle et du changement climatique sur la formation et l'exportation d'eau dense sur le plateau du golfe du Lion. Les outils et la stratégie de modélisation adoptés sont présentés dans la partie 9.2. Les effets de la variabilité atmosphérique interannuelle sont étudiés dans la partie 9.3, où nous quantifions la formation et l'exportation d'eau dense pour un groupe d'années de la période actuelle. Les aspects géographiques de l'exportation sont également examinés, et les résultats obtenus en termes de volumes et de localisation sont comparés avec les observations disponibles. Une quantification et une interprétation des effets du changement climatique sont proposées dans la partie 9.4, où nous étudions la formation et l'exportation d'eau dense pour un groupe d'années à la fin du XXI^e siècle. Les résultats obtenus pour les deux groupes d'années dans les parties 9.3 et 9.4 sont extrapolés à l'ensemble des 30 années de chaque période correspondante, actuelle et future. Les incertitudes de cette étude sont examinées dans la partie 9.6.

La méthode de modélisation utilisée par *Somot et al.* [2006] est rappelée dans le **paragraphe 9.2.1** : le modèle climatique océanique régional (ORCM) OPAMED8 est forcé à la surface par le modèle climatique atmosphérique régional (ARCM) ARPEGE-Climat, sur toute la zone méditerranéenne. Ces deux modèles régionaux sont forcés par un modèle climatique global couplé océan-atmosphère (OAGCM). Cette méthode est utilisée pour réaliser une simulation de 140 ans (1960-2100), en suivant les hypothèses du scénario A2 de l'IPCC [IPCC, 2001, International Panel on Climate Change], ce qui permet d'étudier l'impact potentiel du changement climatique dans les principaux bassins méditerranéens. Les effets sur les processus régionaux et côtiers ne sont pas abordés. Dans le chapitre 7, nous avons montré que la résolution de 1/8° de OPAMED8 ne permettait pas de résoudre les processus de méso-échelle, qui jouent un rôle important dans le devenir de l'eau dense en Méditerranée nord-occidentale. L'utilisation du modèle de plus haute résolution SYMPHONIE, forcé aux frontières ouvertes par OPAMED8, permet en revanche de représenter correctement ces processus. Par ailleurs, nous avons montré dans le chapitre 8 qu'augmenter la résolution du forçage atmosphérique améliorait notablement la modélisation océanique dans le golfe du Lion. La résolution de l'ARCM utilisé par *Somot et al.* [2006] est la même que celle du forçage de haute résolution du chapitre 8. Il paraît donc opportun d'utiliser le modèle SYMPHONIE, forcé aux limites par les résultats de l'ORCM OPAMED8 et de l'ARCM ARPEGE-Climat, afin d'étudier le processus de *cascading* dans le golfe du Lion. Pour des raisons techniques, il n'est cependant pas possible d'effectuer une simulation de 140 ans avec SYMPHONIE. Deux groupes de 7 années sont donc sélectionnés dans les périodes actuelle (1961-1990) et future (2071-2100) à partir de flux atmosphériques hivernaux de chaleur. Le principe de cette sélection est expliqué dans le paragraphe 9.2.1. 14 simulations régionales sont effectuées avec SYMPHONIE, correspondant aux 14 années sélectionnées. Les 140 ans de la simulation de grande échelle parmi lesquels sont sélectionnées ces années correspondent à la réalité d'un point de vue climatologique, mais pas d'un point de vue chronologique (par exemple, l'année 1967 correspond uniquement à la 8^{ème} année de cette simulation).

Le paragraphe 9.2.2 rappelle les caractéristiques du modèle SYMPHONIE et du forçage aux limites.

Pour étudier la formation et l'exportation d'eau dense sur le plateau du golfe du Lion au moyen des 14 simulations numériques, nous délimitons ensuite une frontière (SDS, voir Fig. 9.2) dans le paragraphe 9.2.3, ainsi qu'un critère de densité : la densité à 1000 m de fond au mois de décembre le long de la frontière SDS, à laquelle est ajoutée une valeur constante, est choisie comme critère de densité.

L'effet de la variabilité atmosphérique interannuelle est d'abord étudié pour le climat actuel, dans la partie 9.3. Nous étudions pour cela la formation (paragraphe 9.3.1), l'élimination par mélange (paragraphe 9.3.2) et l'exportation (paragraphe 9.3.3) d'eau dense (Fig. 9.4), ces trois processus étant largement corrélés (85%, 85% et 83%) avec les conditions atmosphériques hivernales, à savoir la perte de chaleur à la surface pendant la période de formation, qui s'étend de décembre à mars, HL_{DJFM} . La variabilité interannuelle est très forte pour les trois processus, avec un facteur d'environ 20 entre les années les plus productives et les années les moins productives. Pendant les années froides, les importants volumes d'eau dense formés sont encore augmentés par le phénomène de mélange, en raison de la haute densité des masses d'eau sur le plateau due aux fortes pertes de chaleur en surface, et sont majoritairement éliminés du plateau par exportation vers le large (60% à 85%), le reste étant éliminé par mélange après la période de formation. 50% à 60% de l'eau exportée coule vers le fond de l'océan pendant ces années froides, majoritairement à travers le Canyon du Cap Creus (Fig. 9.6), et le reste de l'eau exportée continue à circuler dans les premiers 200 mètres de profondeur en suivant la côte vers l'Espagne. Nous définissons alors le *cascading* comme la partie de l'exportation ayant lieu sous 200m de profondeur. Les volumes ainsi exportés vers le fond varient entre 300 km³ et 800 km³. Pendant les années chaudes, les faibles pertes de chaleur induisent une plus faible augmentation de la densité des masses d'eau sur le plateau. En raison de cette plus basse densité, les faibles volumes d'eau dense formés sont entièrement consommés par le mélange avec les eaux avoisinantes sur le plateau, et n'ont pas le temps d'atteindre le talus continental. L'infime quantité d'eau qui traverse la frontière reste en sub-surface en suivant la côte.

Les résultats obtenus pour ces 7 années sont comparés avec les observations disponibles dans le paragraphe 9.3.4 : les caractéristiques de l'exportation modélisée ici sont en accord avec ces observations en termes de quantité d'eau dense exportée, de contraste de densité, de vitesses de courant et de localisation géographique.

La méthode de modélisation adoptée dans cette étude donne des résultats satisfaisants pour le climat actuel, il paraît donc légitime **d'appliquer cette méthode au climat futur pour étudier les éventuels effets du changement climatique. Ceci fait l'objet de la partie 9.4.**

Dans cette partie, nous étudions pour chaque année sélectionnée dans la période future la formation, l'élimination et l'exportation d'eau dense (Fig. 9.7). La période de formation est la même qu'en climat actuel (fin décembre - mars), et la variabilité interannuelle est encore très forte.

La principale différence entre le climat actuel et la fin du XXI^e siècle concerne les volumes formés, exportés, et cascadant vers le fond. Sur l'ensemble des années étudiées, on note une diminution de 50% de la quantité d'eau formée. La proportion

d'eau formée qui quitte le plateau diminue nettement par rapport aux années de la période actuelle : les années où l'exportation n'est pas négligeable, elle représente 15% à 50% du volume d'eau dense formée, contre 60% à 85% pour les années de la période actuelle. L'eau dense est majoritairement éliminée par mélange dans la période future. Enfin, l'exportation vers l'océan profond n'a lieu qu'une année, et ne représente que 8% de l'exportation totale, contre 50% à 60% pour les années froides du présent (Fig. 9.6). La quantité absolue d'eau dense exportée vers le fond pour cette année est d'un ordre de grandeur inférieure à celle des années froides de la période actuelle.

Contrairement à ce que l'on pourrait penser, cette diminution de la formation et de l'exportation d'eau dense n'est pas due à une diminution de la perte de chaleur à la surface pendant la période hivernale. Au contraire, celle-ci augmente même en moyenne entre la période actuelle et la fin du XXIème siècle (Fig. 9.1 et 9.8). En revanche, dans la simulation de *Somot et al.* [2006], la perte de chaleur annuelle diminue au cours du XXIème siècle, entraînant une augmentation de la stratification entre la fin du XXème et du XXIème siècles. Cette augmentation de stratification est à l'origine de la diminution de la formation et de l'exportation d'eau dense.

Pour quantifier l'effet de la stratification, nous calculons la perte de chaleur HL_{strat} nécessaire pour augmenter la densité de l'eau initialement sur le plateau en décembre jusqu'au critère de densité. Nous effectuons ce calcul sur les 30 années des périodes actuelle et future en utilisant les résultats de l'ORCM, et nous obtenons les moyennes actuelle et future de la perte de chaleur liée au gradient de densité vertical le long de la frontière, $HL_{strat,p}$ et $HL_{strat,f}$. Comme le critère de densité dépend de la densité à 1000 m le long de la frontière en décembre, $HL_{strat,f}$ est plus importante que $HL_{strat,p}$ ($\sim +30 \text{ W.m}^{-2}$), traduisant le fait qu'à perte de chaleur atmosphérique égale, il est plus difficile pour l'eau présente sur le plateau d'atteindre le critère de densité à la fin du XXIème siècle que pendant la période actuelle. Ceci explique la diminution de la formation d'eau dense à la fin du XXIème siècle. Comme nous l'avons vu dans le paragraphe 9.3.2, la diminution du volume favorise de plus l'élimination de l'eau dense par mélange. Par ailleurs, la plus forte stratification explique que la densité des eaux avoisinantes par rapport au critère de densité soit plus faible dans la période future, ce qui augmente encore l'élimination par mélange.

L'augmentation de la stratification est donc responsable de la diminution de la formation d'eau dense d'ici la fin du XXIème siècle, et de la diminution de la proportion d'eau éliminée par le transport vers le large. Enfin, elle entraîne également une diminution du contraste entre la densité de l'eau dense qui réussit à atteindre la frontière et les eaux avoisinantes, comme observé sur la Fig. 9.3. Ceci explique que l'eau dense qui atteint la frontière soit moins facilement exportée vers l'océan profond (Fig. 9.6). Finalement, pour les années sélectionnées, le phénomène de *cascading* diminue d'au moins 90% entre le XXème siècle et la fin du XXIème siècle.

Les résultats obtenus pour les années sélectionnées dans les périodes actuelle et future dans les parties 9.3 et 9.4 sont extrapolés à l'ensemble de 30 années des deux périodes dans la partie 9.5. Pour cela, nous utilisons les corrélations entre les quantités d'eau dense formée, exportée et cascadiant chaque année et la perte de chaleur hivernale. Cependant, comme nous l'avons vu dans la partie 9.4 et sur la Fig. 9.8, ces volumes ne sont pas corrélés uniquement à la perte de chaleur atmosphérique hivernale HL_{DJFM} , mais aussi à la stratification.

Plutôt que de chercher une relation entre les différents volumes annuels d'eau dense et HL_{DJFM} , nous relierons ces volumes avec la différence entre la perte de chaleur atmosphérique hivernale et la perte de chaleur liée à la stratification, HL_{strat} . Cette différence, HL_{eff} , correspond en quelque sorte à la perte de chaleur réellement utilisée pour produire de l'eau dense à la surface. Nous établissons une relation du type $y = f(x) = ax + b$ entre la formation à la surface annuelle et HL_{eff} (Fig. 9.9a). En revanche, ayant observé dans la partie 9.3 que l'eau dense était exportée et cascadaient uniquement pour les années plus froides que la moyenne, vérifiant donc $HL_{eff} > \overline{HL}_{eff,p}$, où $\overline{HL}_{eff,p} = \overline{HL_{DJFM}} - \overline{HL_{strat,p}}$ est la moyenne sur la période actuelle de HL_{eff} , nous établissons une relation du type $y = f(x) = ax$ entre l'exportation et le *cascading* annuels (y) et $x = HL_{eff} - \overline{HL}_{eff}$ (Fig. 9.9b,c). Les régressions obtenues sont ensuite appliquées à chacune des 30 années des deux périodes, et la moyenne sur chaque période fournit une estimation de la formation, de l'exportation et du *cascading* annuels d'eau dense moyens pour le XXème siècle et la fin du XXIème siècle. Pour les deux périodes, et pour les trois types de volumes, la variabilité interannuelle, représentée par l'écart type sur l'ensemble des 30 années, est très forte. Pour le climat actuel, nous obtenons respectivement 800 km³, 600 km³ et 300 km³ pour la formation, l'exportation et le *cascading* annuels moyens. Ces volumes sont réduits respectivement de 50%, 90% et 90% à la fin du XXIème siècle.

Nous examinons dans la partie 9.6 les incertitudes sur les résultats obtenus dans la partie 9.5. Pour cela, nous étudions la sensibilité de ces résultats au critère d'eau dense, au modèle atmosphérique utilisé pour forcer OPAMED8 et SYMPHONIE à la surface, à la variabilité naturelle du climat et au choix du scénario de changement climatique.

L'impact du choix du critère de densité est examiné dans le paragraphe 9.6.1 en utilisant les valeurs obtenues pour différents critères pour les deux groupes d'années sélectionnées. Ce critère a un impact non négligeable sur les valeurs absolues des quantités annuelles d'eau dense exportée. Cependant, l'impact du choix du critère sur le rapport entre les valeurs obtenues pour les différentes années sélectionnées est négligeable, tant sur la période actuelle que sur la période future. Les conclusions formulées dans les parties précédentes sur les impacts relatifs de la variabilité atmosphérique interannuelle et du changement climatique ne dépendent donc pas du critère choisi.

Dans le paragraphe 9.6.4, nous utilisons les résultats du projet PRUDENCE, dans le cadre duquel des études climatiques ont été menées avec différents ARCM pour les périodes 1961-1990 et 2071-2100, suivant les hypothèses des scénario A2 et B2 de l'IPCC. Nous montrons que l'impact du choix de l'ARCM utilisé pour forcer OPAMED8 et SYMPHONIE est relativement important. Cependant, quel que soit l'ARCM, le passage de la période actuelle à la période future s'accompagne d'une diminution d'au moins 30%, 50% and 50% des quantités annuelles respectives d'eau dense formée, exportée du plateau et exportée vers le fond, lorsqu'on utilise les hypothèses du scénario A2. Ces conclusions diffèrent dans le scénario B2, où les volumes annuels augmentent même selon certains ARCM. La sensibilité des résultats à la résolution spatiale de l'ARCM, à l'AOGCM et à la variabilité du climat est nettement moins importante. Il faut noter que l'ORCM n'a pas été forcé chaque ARCM, en raison notamment de l'énorme coût informatique que cela représenterait. Nous

avons donc considéré que la stratification était donnée pour les deux périodes par la simulation OPAMED8 forcée par l'ARCM ARPEGE-Climat. L'incertitude liée à la stratification obtenue en utilisant différents ARCM est certainement importante, il n'est cependant pas possible de l'évaluer pour le moment en raison du manque de simulations réalisées avec le même ORCM forcé par différents ARCM.

Les résultats de cette étude sont résumés dans la partie 9.7, ainsi que ses limitations et les perspectives possibles. En étudiant deux groupes d'années, l'un pour le climat du XXème siècle, l'autre pour la fin du XXIème siècle, et en extrapolant les résultats obtenus à l'ensemble des 30 années de chaque période, nous avons examiné les effets de la variabilité atmosphérique interannuelle et du changement climatique sur la formation, l'exportation et le *cascading* d'eau dense sur le plateau du golfe de Lion.

Dans les conditions climatiques actuelles, la variabilité de ces processus est forte, et les volumes d'eau dense formée, exportée et cascadiant sont fortement liés à la variabilité de la perte de chaleur atmosphérique hivernale, avec des valeurs annuelles moyennes respectivement de 800 km³, 600 km³ et 300 km³. La formation d'eau dense a lieu chaque année, mais l'exportation et le *cascading* n'ont lieu que pour les hivers plus froids que la moyenne, environ une année sur deux.

A la fin du XXIème siècle, le renforcement de la stratification induit par la diminution de la perte de chaleur annuelle explique la diminution de la formation, de l'exportation et du *cascading* d'eau dense de respectivement 50%, 90% et 90%. Des quantités significatives d'eau dense ne sont exportées que pour 2 années sur 30 dans la période future. Une telle évolution aurait très certainement un impact non négligeable sur le fonctionnement des écosystèmes profonds. Par ailleurs, le *cascading* d'eau dense en provenance du plateau ne semble pas constituer une alternative envisageable à la formation d'eau dense lors de la convection profonde au large.

Ces résultats sont sensibles à l'ARCM utilisé ainsi qu'au scénario de changement climatique. Cependant, sous les hypothèses du scénario A2, tous les ARCM prédisent une diminution notable de la formation et de l'exportation d'eau dense.

Etant donnés les progrès technologiques actuels, il sera certainement possible prochainement d'effectuer deux fois 30 années de simulations avec SYMPHONIE, pour les périodes actuelle et future. Ceci permettrait d'affiner les résultats obtenus ici, notamment en ce qui concerne la variabilité interannuelle, et d'éviter de recourir à des méthodes d'extrapolation, mais aussi de confirmer les relations obtenues entre la perte de chaleur à la surface, les volumes d'eau dense annuels et la stratification. Par ailleurs, il serait très intéressant d'effectuer des simulations avec OPAMED8 forcé par les différents ARCMs, afin d'évaluer l'incertitude liée à la stratification. En effet, on peut s'attendre à ce que la stratification varie d'un modèle à l'autre, notamment en ce qui concerne la fin du XXIème siècle. Ce changement de stratification étant le principal responsable du changement du taux annuel de formation, d'exportation et de *cascading*, on peut s'attendre à ce que les conclusions formulées en ce qui concerne l'impact du changement climatique varient d'un modèle à l'autre en fonction de la stratification obtenue. Il ne serait pas nécessaire d'effectuer de nouvelles simulations avec SYMPHONIE pour chaque ARCM, et l'on pourrait utiliser les relations obtenues entre les volumes d'eau dense, la perte de chaleur à la surface et la stratification. Des simulations réalisées avec un ORCM forcé par plusieurs ARCMs devraient cependant être disponibles prochainement grâce au projet européen CIRCE

(<http://www.bo.ingv.it/circeip/>). Enfin, les observations réelles quantitatives de *cascading* restent limitées, sans parler de l'observation de l'évolution de ce processus au cours des dernières décennies. De telles observations permettraient d'améliorer la modélisation de ce processus dans les conditions climatiques actuelles, rendant ainsi plus fiables les conclusions obtenues pour la fin du XXIème siècle.

ARTICLE PUBLIE A *CONTINENTAL SHELF RESEARCH*
doi :10.1016/j.csr.2008.03.003

Dense water formation in the Gulf of Lions shelf : impact of atmospheric interannual variability and climate change

Auteurs : M. Herrmann, C. Estournel, M. Déqué, P. Marsaleix, F. Sevault et S. Somot.

Dense water formed over the continental shelf and cascading down the slope is responsible for shelf-slope exchanges in many parts of the world ocean, and transports large amounts of sediment and organic matter into the deep ocean. Here we perform numerical modeling experiments to investigate the impact of atmospheric interannual variability and climate change on dense water formation over the Gulf of Lions shelf, in the Northwestern Mediterranean Sea. Results obtained for a 140 years eddy-permitting simulation (1960-2100) performed over the whole Mediterranean sea under IPCC A2 scenario forcings are used to force a regional eddy-resolving model of the Northwestern Mediterranean Sea.

For the years selected in the present period, the quantity of dense water formed over and exported from the shelf is well correlated with atmospheric conditions, and dense water cascading is in agreement with available observations. During years colder than the average, most of the dense water formed over the shelf sinks into the deep ocean by cascading. During warmer years, dense water is mainly consumed by mixing with lighter surrounding water, and only a small quantity escapes the shelf, flowing along the coast without sinking.

For the years selected in the future period, dense water formation over the shelf is strongly reduced, due to the stronger stratification of the water column. Most of the dense water formed is consumed over the shelf by mixing. A very small part escapes the shelf, flowing mainly in the surface layer : cascading practically disappears.

The extrapolation of the results obtained for the selected years to the whole present and future periods suggests that volumes of dense water annually formed on the shelf, exported and cascading from the shelf are reduced by respectively 50%, 90% and 90% between the 20th century and the end of the 21st century. Uncertainties regarding our results are evaluated : the uncertainty due to the choice of the atmospheric forcing model is the most important, however, a decrease of cascading of at least 60% for the end of the 21st century compared to the present climate is obtained for every atmospheric model examined.

9.1 Introduction

In some parts of the world ocean coastal regions, winter atmospheric conditions induce episodic formation over the shelf of water of greater density than adjacent waters over the slope [Shapiro and Hill, 1997; Ivanov *et al.*, 2004]. This water cascades down the shelf-open ocean slope, transporting irreversibly large amounts of

sediment and organic matter into the deep ocean, thus contributing to deep ocean carbon storage. Since it is strongly driven by atmospheric conditions, dense water (DW) cascading process shows a high interannual variability [Huthnance, 1995]. Due to its relative ease of access, the Gulf of Lions shelf, in the Mediterranean Sea, is particularly appropriate to study DW cascading. Several cascading events were observed during the last decades in this region [Béthoux *et al.*, 2002a; Durrieu de Madron *et al.*, 2005; Canals *et al.*, 2007], where the shelf-open ocean slope is cut by several canyons that funnel DW cascading down the slope. Due to the presence of the Rhône river, continental input and biological productivity over the Gulf of Lions shelf are high. DW cascading contributes importantly to the transport of this sediment and organic matter into the deep ocean, therefore affecting geological characteristics and deep ecosystems functioning in this area [Monaco *et al.*, 1990; Palanques *et al.*, 2006; Gaudin *et al.*, 2006; Heussner *et al.*, 2006; Canals *et al.*, 2007]. Due to its intermittent character, cascading is difficult to observe and its contribution to shelf - deep ocean exchanges is difficult to quantify. However, analysing series of sediment concentration, hydrological characteristics and current velocity provided by moorings equipped with current meters and sediment traps and installed in the canyons of the Gulf of Lions, the experimentators cited above estimated volumes of DW water and organic matter transported along the slope for winters 1998-99 and 2004-05 and for the 1993-2001 period. The first experimental study aimed at describing spatial, seasonal and interannual variability of the flux intensity of particulate matter was performed by Heussner *et al.* [2006]. They concluded that DW cascading may be predominantly responsible for the interannual variability of the transfer of particulate matter. However, they underlined that causal relationships between the forcings and this variability could not be demonstrated by the time series analyzed, and that further studies of such relationships are necessary.

Beside these observations, numerical studies of observed cascading events were performed by Dufau-Julliand *et al.* [2004] and Ulses *et al.* [2008] for winters 1998-99 and 2003-2004 using the numerical circulation model SYMPHONIE. Those studies demonstrated the ability of this model to reproduce correctly DW formation and cascading characteristics, in particular the DW formation areas, the cascading velocities, the volume of cascading water and the intermittence of the cascading process. SYMPHONIE can therefore be used now to examine the interannual variability of the cascading process and to provide further quantification of integrated DW fluxes. This would help to complete the observational study performed by Heussner *et al.* [2006] and to provide a first answer to the issues raised by these authors. This constitutes the first objective of the present study.

Somot *et al.* [2006] showed that climate change could reduce open-ocean convection and associated DW formation in the Mediterranean Sea. Given the high sensitivity of DW cascading to meteorological conditions, one can expect this process to be influenced by climate change. A numerical model is used here to provide a first answer to this question, to raise the important issues that need to be studied and to evaluate the uncertainties of climate change impact.

We perform a three-dimensional numerical study in order to investigate the effects of atmospheric interannual variability and climate change on DW formation over and export off the Gulf of Lions shelf. The modeling tools and strategy are presented in Section 9.2. In Section 9.3 we examine the effects of atmospheric interannual variability under present climate conditions by studying a group of selected years.

Quantitative estimations of the volumes of DW formed over the shelf then exported and cascading, and of their interannual variability, are proposed and compared with available data. We also study the geographical characteristics of DW export and cascading. Impacts of climate change on these volumes and characteristics are examined and quantified for a group of selected years in Section 9.4, and explanations for these impacts are proposed. Results obtained in Sections 9.3 and 9.4 are extrapolated to the whole present and future periods in Section 9.5. Uncertainties regarding our results are presented in Section 9.6.

9.2 Tools and methods

9.2.1 Modeling strategy

Somot et al. [2006] performed a 140-year (1960-2100) numerical study over the whole Mediterranean Sea to investigate the impact of climate change on the Mediterranean thermohaline circulation. For that, they used the $1/8^\circ$ resolution Oceanic Regional Circulation Model (ORCM) OPA, eddy-permitting in the NWMS. To force this model at the surface, air-sea fluxes were provided by a run performed with the high-resolution (50 km) Atmospheric Regional Climate Model (ARCM) ARPEGE-Climate over the 1960-2100 period [*Gibelin and Déqué*, 2003]. Both the ARCM and the ORCM were forced by the results of a simulation performed with the low-resolution Atmosphere-Ocean General Circulation Model (AOGCM) ARPEGE-OPA. These simulations were divided into two periods. During the first period (1960-2000), the greenhouse gases and aerosols concentrations corresponded to the observed concentrations. During the second period (2000-2100), these concentrations increased following the IPCC A2 scenario [IPCC, 2001]. Note that there was no data assimilation in the atmospheric simulations : they were realistic from a climatological point of view, but, due to the atmospheric chaotic behavior, a climate model year did not correspond to the actual year with the same number. For example, year number 1962 is just the third year of the simulation, and one should not expect this year to follow the chronology of the real year 1962. In the ORCM simulation, a surface relaxation toward the AOGCM sea surface temperature (SST), used to force the ARCM, ensured the consistency between surface heat fluxes coming from the ARCM and SST calculated by the ORCM. This term, equivalent to a heat flux, and called the relaxation heat flux in the following, was actually a first-order coupling between the ORCM SST and the atmosphere heat flux.

Somot et al. [2006] showed that climate change could reduce open-ocean convection and associated DW formation in the Mediterranean Sea main basins by the end of the 21st century. However, effects of climate change on regional and coastal processes like shelf DW formation were not examined. *Herrmann et al.* [2008b] showed that $1/8^\circ$ resolution is not sufficient to simulate correctly the mesoscale processes involved in the NWMS circulation but that using an embedded eddy-resolving model enables to represent accurately such processes, that play an important role in the fate of DW. Results of the ORCM and ARCM simulations are therefore used here to prescribe surface and lateral open boundary conditions for the regional eddy-resolving oceanic model described in Section 9.2.2, in order to study the impacts of atmospheric interannual variability and climate change on the DW formation and export over the Gulf of Lions shelf.

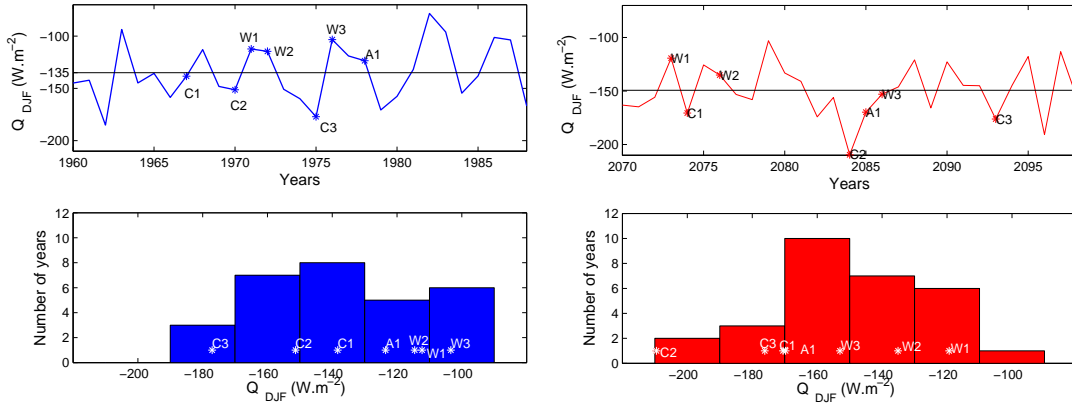


FIG. 9.1 – Selection of representative years in the present (left) and future (right) periods. Top : winter heat flux averaged over the NWMS in the ARCM simulation, $Q_{DJF} = -HL_{DJF}$. The black line corresponds to the winter heat loss averaged over the whole period. Bottom : distribution of Q_{DJF} in the ARCM simulation. Value of Q_{DJF} for each selected year is marked by an asterisk and the corresponding year name.

Due to technical constraints, it is not currently possible to perform a 140-year numerical simulation with the regional eddy-resolving oceanic model. The strategy adopted here is therefore to select a set of representative years for the 20th century (1961-1990, the “present period”) and for the end of the 21st century (2071-2100, “the future period”) in the 140-year simulation. We choose the 1961-1990 and 2071-2100 periods, long enough to ensure a large signal/noise ratio : the climate change signal will not be masked by the natural variability of the climate system. Since DW formation is strongly influenced by winter surface heat loss, we examine surface heat loss averaged over the coldest period, i.e. December - February, HL_{DJF} , and over the NWMS, for each year of the 30-year present and future periods of the ARCM simulation (Fig. 9.1). Note that HL_{DJF} is in average stronger for the future period (150 W.m^{-2}) than for the present period (135 W.m^{-2}). Seven years are selected for each period, with winter heat loss distributed over the whole range of the heat loss values (see the histograms on Figure 9.1) : three years with strong heat loss (“cold years”, C1, C2, C3), three years with weak heat loss (“warm years”, W1, W2, W3) and an approximately average year (A1). The regional oceanic model is then used to perform 14 one-year simulations over the NWMS, corresponding to the 14 selected years. Each simulation begins in September.

9.2.2 The numerical eddy-resolving regional oceanic model

The 3D primitive equation hydrostatic ocean model SYMPHONIE is described in detail in *Marsaleix et al.* [2006]. The model configuration used here is the same as the one described in *Herrmann et al.* [2008b]. Previous studies showed that this model reproduces correctly the shelf DW formation in the Gulf of Lions [*Dufau-Julliand et al.*, 2004; *Ulses et al.*, 2008] and in the Gulf of Thermaikos [*Estournel et al.*, 2005] as well as the open-sea deep convection in the Northwestern Mediterranean Sea [*Herrmann et al.*, 2008b; *Herrmann and Somot*, 2008].

Due to the hydrostatic assumption, the model does not represent the convective processes that restore the stability in the real ocean when static instabilities develop. Therefore, to take those processes into account, a non-penetrative convective adjustment algorithm, as described by *Madec et al.* [1991a], is used in case of unstable stratification. The use of a hydrostatic model could be questionable here since strong variations of current are likely to be found through the head of the DW plumes. *Heggenlund et al.* [2004] showed that the shape of the DW plume head is quite sensitive to the choice of a hydrostatic or non-hydrostatic model, but that the thickness of the plume behind the head and the time required for the DW to reach the depth of buoyancy equilibrium are nearly the same in both cases. As far as we are more concerned with global issues than in the plume dynamics itself, the use of a hydrostatic model is therefore acceptable. Moreover, the computation of the non-hydrostatic pressure elliptic equation is quite expensive. For the same cost, the hydrostatic model has a better resolution and/or a larger domain and represents consequently better the background circulation that plays a significant role in the DW fate [*Shapiro and Hill*, 1997; *Dufau-Julliand et al.*, 2004]. Fig. 9.2 shows the modeled domain.

For each selected year, lateral boundary conditions for SYMPHONIE are provided at each time step by the time-interpolated monthly averaged outputs of the corresponding year in the ORCM simulation performed by *Somot et al.* [2006]. The ORCM simulation also provides the September initial conditions for each selected year. At the surface, the model is forced by daily air-sea fluxes extracted from the ARCM run : heat flux, water flux and wind stress. The value of the relaxation heat flux applied in the ORCM simulation is added to the ARCM heat flux. The freshwater discharge of the Rhône river is introduced as a lateral boundary condition, using the same values as *Somot et al.* [2006] : the UNESCO RivDis database [*Vörösmarty et al.*, 1996] provides climatological monthly values for the discharge during the present period. For the future period, they apply for each decade a constant multiplying factor to those climatological monthly values in order to modify the Rhône runoff accordingly to the ARCM simulation hydrological fluxes. The consistency of this forcing method was demonstrated in the process study performed by *Herrmann et al.* [2008b], that showed that SYMPHONIE does not drift away from the ORCM.

9.2.3 Dense water criteria

In the following, the boundary between the shelf and the deep sea (SDS boundary) is defined using the 1000m isobath that runs across the slope (see Fig. 9.2). It is then necessary to establish a consistent density criteria to distinguish DW formed over the shelf and crossing this boundary from the surrounding water. Since cascading DW has variable density characteristics from one year to another [*Béthoux et al.*, 2002a], it would not be adequate to use a unique value. Moreover, as we will see in the following, water density over the Gulf of Lions shelf and along the SDS boundary changes a lot between the end of the 20th and 21st centuries (Fig. 9.3). Examining the density over the vertical section formed by the SDS boundary, DW cascading can be identified when flows of water of higher density than the surrounding water flow across the boundary, as observed on a vertical section of the density in the Cap Creus Canyon during cascading events occurring during years C2 of the

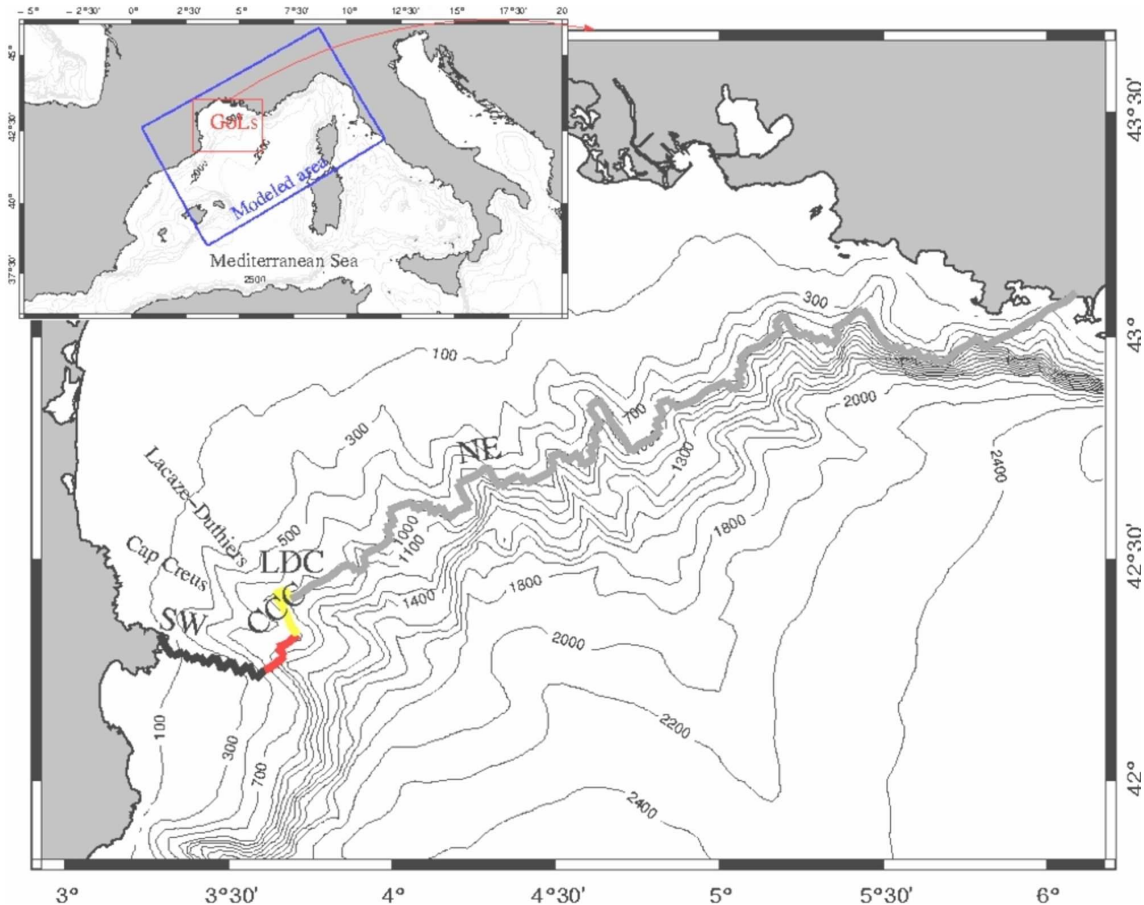


FIG. 9.2 – **Bathymetry of the modeled domain** (unit : m). The blue box in the small frame shows the boundaries of the area covered by the regional oceanic model SYMPHONIE. The red box correspond to the zoomed area for which the bathymetry is shown. The colored (black, red ...) line in the large frame represents the shelf-deep sea (SDS) boundary, with the colors corresponding to the portions detailed in Section 9.3.3 (black : Southwestern end, red : Cap Creus canyon, yellow : Lacaze-Duthiers canyon, grey : Northeastern end).

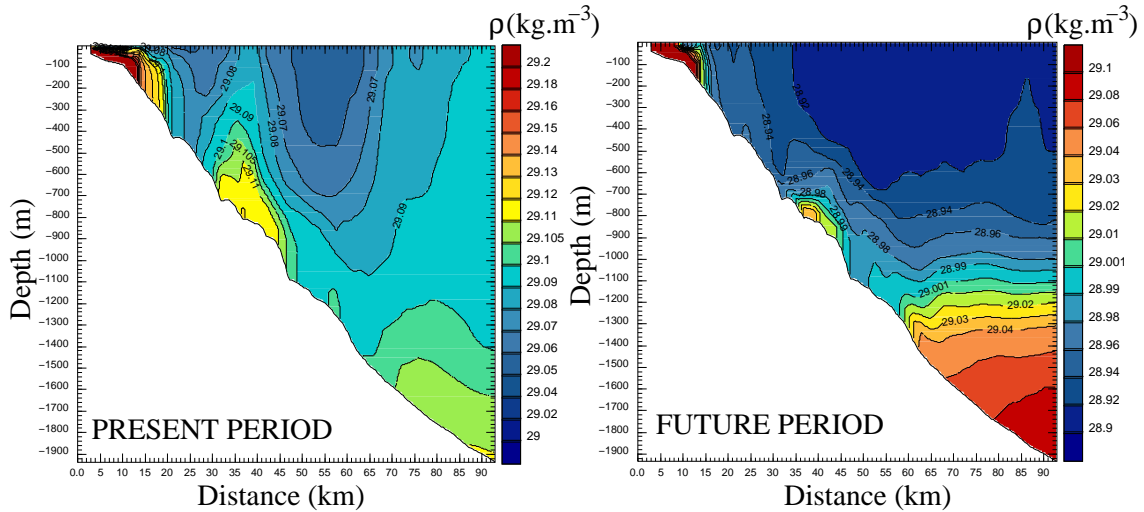


FIG. 9.3 – Density (kg.m^{-3}) along the Cap Creus canyon during cascading events. Left : in the present period (C2, $\rho_{bottom} = 29.075 \text{ kg.m}^{-3}$, $\rho_{crit} = 29.105 \text{ kg.m}^{-3}$). Right : in the future period (C2, $\rho_{bottom} = 28.701 \text{ kg.m}^{-3}$, $\rho_{crit} = 29.001 \text{ kg.m}^{-3}$).

present and future period (Fig. 9.3). The density criteria is therefore defined as $\rho_{crit} = \rho_{bottom} + \Delta\rho$. ρ_{bottom} is the mean density at the bottom of the SDS boundary averaged over the month preceding potential cascading events, i.e. December. $\Delta\rho$ is a constant density anomaly corresponding to the difference between the DW that escapes the SDS boundary and the water present at the bottom of this boundary. The value of $\Delta\rho$, here 0.03 kg.m^{-3} , is determined by examining the density over the boundary when cascading occurs (see for example Fig. 9.3). Moreover, this value seems to give realistic results when estimating the quantity of DW cascading across the slope, as we will see in Section 9.3.4. The obtained criteria is presented in Table 9.1. A sensitivity analysis to this criteria is presented in Section 9.6.

9.3 Impact of interannual variability on the dense water formation and transport under present-day climate conditions

In this section, we investigate the effects of interannual variability on DW formation over and export from the Gulf of Lions shelf. For this purpose, we compare the results obtained for the seven years selected in the present period. In the following, the region used to compute volumes or surfaces over the shelf is the region located northwest of the SDS boundary shown on Fig. 9.2. DW formation does not occur before December, we therefore examine the evolution of the DW formed over the shelf after December 1st of each year. DW can be formed or consumed by surface fluxes, stored over the shelf, formed or eliminated by mixing or by advection across the SDS boundary, following the conservation equation

$$V = Surf + Mix + Trans \quad (9.1)$$

TAB. 9.1 – Density of water over the shelf during the DW formation period (20/12 - 01/04) for each selected year of the present and future periods, average ($\bar{\rho}$) and standard deviation (σ_{ρ}). Dense water criteria ρ_{crit} , temporal maximum of the water density averaged over the shelf, $\rho_{GDL,max}$, and temporal maximum of the mean density of light water surrounding the DW (corresponding to $\rho < \rho_{crit}$), $\rho_{LW,max}$. Unit : kg.m⁻³

	C1	C2	C3	A1	W1	W2	W3	$\bar{\rho}$	σ_{ρ}
PRESENT PERIOD									
ρ_{crit}	29.103	29.105	29.110	29.108	29.107	29.105	29.112	29.107	0.003
$\rho_{GDL,max}$	29.07	29.07	29.08	28.99	28.96	28.91	29.00	29.01	0.06
$\rho_{LW,max}$	29.02	29.03	29.03	28.97	28.94	28.91	28.97	28.98	0.05
FUTURE PERIOD									
ρ_{crit}	28.993	29.001	28.985	28.991	29.001	28.996	29.992	28.994	0.006
$\rho_{GDL,max}$	28.90	28.93	28.73	28.90	28.86	28.67	28.76	28.82	0.10
$\rho_{LW,max}$	28.88	28.87	28.72	28.85	28.84	28.67	28.76	28.80	0.08

where $Surf$ is the volume of DW formed at the surface, V is the stored volume, Mix is the volume formed by mixing and $Trans$ is the net volume transported across the boundary into the shelf. Positive (resp. negative) values for $Surf$, Mix and $Trans$ correspond to production (resp. consumption) of DW over the shelf. For each year, the volume $\Delta Surf$ of DW produced at the surface by the atmospheric fluxes during the time Δt is computed using the *Walsh* [1982] method as done by *Tziperman* [1986] and *Speer and Tziperman* [1992] : this volume corresponds to the volume of water that crosses the isopycnal ρ_{crit} due to the surface fluxes. It can be evaluated using the *Speer and Tziperman* [1992] formula :

$$\Delta Surf = \frac{-\rho_0}{g\delta\rho} \sum_{(x,y)/\rho(x,y) \in [\rho_{crit} \pm \frac{1}{2}\delta\rho]} B \Delta x \Delta y \Delta t \quad (9.2)$$

with $g = 9.81$ m.s⁻² the gravitational acceleration, $\rho_0 = 1020$ kg.m⁻³ the density reference, $\Delta x = \Delta y = 3000$ m the model resolution and $\delta\rho = 0.01$ kg.m⁻³. As explained by those authors, the value of $\delta\rho$ is a compromise : it should be small enough so that one does not include a too large range of density values, but large enough not to exclude grid points containing DW because of the averaging induced by the model resolution. We performed sensitivity test to $\delta\rho$ and obtained a 6% range of variation for the volume of DW formed when $\delta\rho \in [0.002; 0.05]$ kg.m⁻³ : $\delta\rho$ is not a significant source of uncertainty in this study. The buoyancy flux B is given by

$$B = g \cdot \left(\frac{\alpha \cdot Q}{\rho_0 \cdot C_p} - \beta \cdot SSS \cdot (E - P) \right) \quad (9.3)$$

where $Q = -HL$ is the mean heat flux during Δt , SSS is the sea surface salinity, $E - P$ is the net water loss, $C_p = 4000$ J.kg⁻¹.K⁻¹ is the specific heat and $\alpha = 2.10^{-4}$ K⁻¹ and $\beta = 7.6 \cdot 10^{-4}$ are the thermal and saline expansion coefficients. Integrating (9.2) between December 1st and t , we obtain $Surf$, the total volume of DW formed at the surface between December 1st and t . We then compute the volume of DW

stored over the shelf, V , and the cumulated net import of DW across the shelf-slope boundary SDS between December 1st and t , $Trans$. The cumulated volume produced by mixing, Mix , is obtained using the conservation equation (9.7). Results are presented on Fig. 9.4.

Differences of the density of water masses over the shelf between the selected years are much larger than differences of density criteria (Table 9.1). In the following, it is therefore legitimate to compare densities among the different years instead of comparing differences between the density and the criteria, as we should rigorously do, to explain the observed differences.

9.3.1 Formation of dense water over the shelf

DW formation occurs mainly between end of December and beginning of April (Fig. 9.4b), in agreement with observations made by *Palanques et al.* [2006]. It is mainly due to surface fluxes, and for some years, to mixing (Fig. 9.4c).

DW surface formation shows a strong interannual variability, with a factor of 17 between the highest (C2) and lowest (W2) yearly integrated surface formation. Since surface formation occurs during strong heat loss events (Fig. 9.4a,b), this variability is mainly related to the atmospheric variability. We indeed obtain a 0.85 correlation factor between the total quantity of DW formed at the surface between December 1st and the end of the formation period, $Surf_{TOT}$, and the mean heat loss over the NWMS between December and March, i.e. when surface formation occurs, HL_{DJFM} . The water density averaged over the shelf, maximum during the surface formation period, is higher for the cold years than for the warm years due to stronger heat losses (Table 9.1). Consequently, during cold winters, the mixing of large amounts of newly formed DW with the surrounding water, itself denser than during mild winters (Table 9.1), produces DW (Fig. 9.4c). On the contrary, during warm winters, the mixing process concerns low quantities of DW and surrounding waters of low density, and results in the consumption of DW.

9.3.2 Elimination of dense water

For every year, some of the DW formed at the surface is stored during the surface formation period (Fig. 9.4c). However, at the beginning of June, all the DW formed at the surface has been completely eliminated from the shelf. The elimination of DW also shows a strong interannual variability : DW can be consumed by mixing or/and by export, and to a lesser extent, by surface fluxes (Fig. 9.4a,c). For the cold years (respectively C1, C2, C3), the largest part of the DW formed at the surface and by mixing leaves the shelf by crossing the SDS boundary : total cumulated export is equal to respectively 64%, 84% and 61% of the total DW surface formation. On the contrary, for the average and warmer years (A1, W1, W2, W3), DW is completely eliminated by mixing. Two reasons explain this difference.

The first reason was explained in the previous section : due to the difference of water density between cold and warm years, mixing consumes DW during warm years, therefore reducing the volume available for export, whereas it produces DW during cold years. Moreover, the contrast between the DW and the surrounding water is reduced by mixing during the warm years, so that the gravity current, i.e. the cascading, resulting from this contrast is slower. DW stays therefore longer over

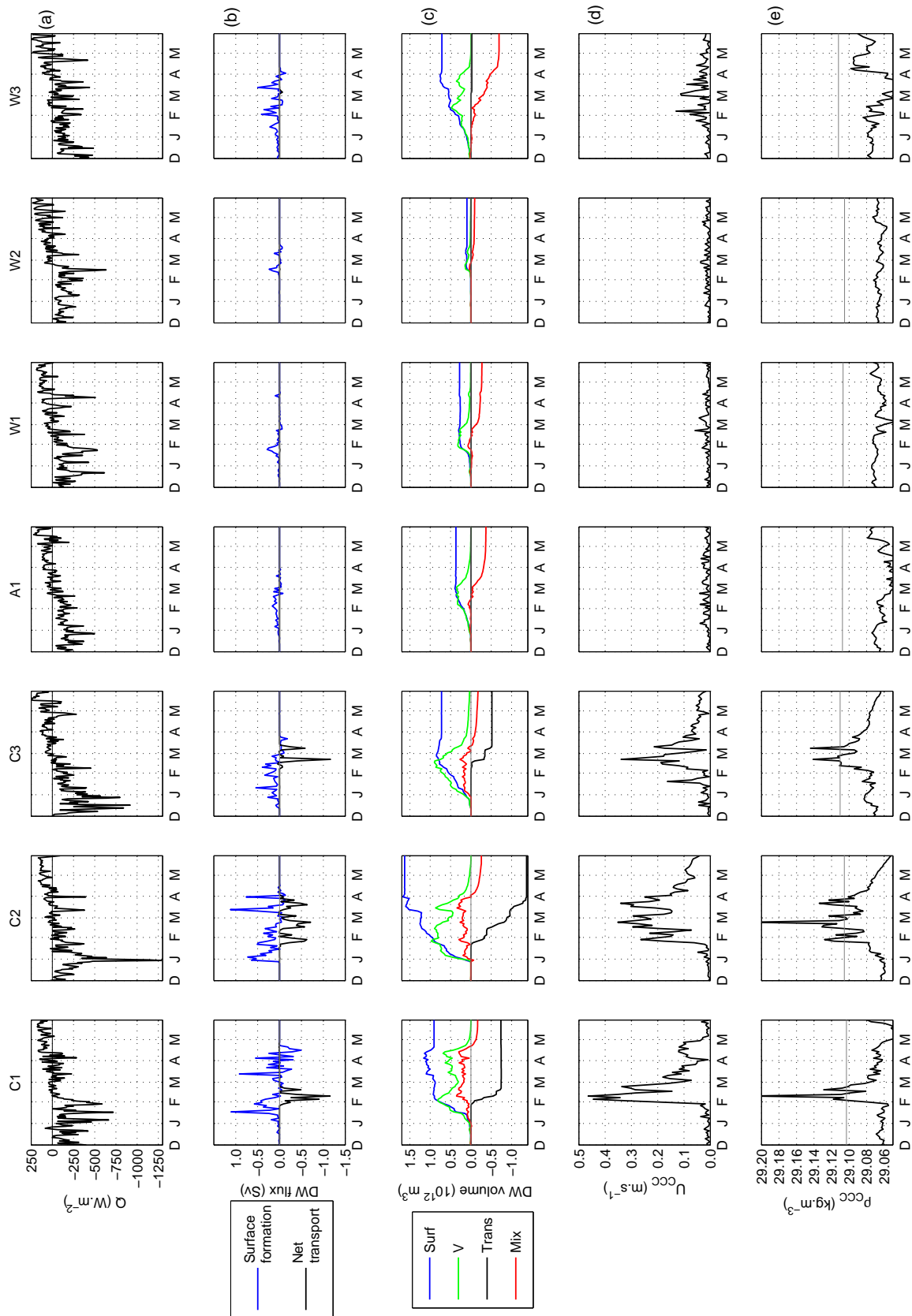


FIG. 9.4 – Evolution of water over the Gulf of Lions shelf during the selected years of the present period. (a) Heat flux, $Q = -HL$, averaged over the NWMS ($\text{W} \cdot \text{m}^{-2}$). (b) DW surface formation (blue) and net transport (black) across the shelf-slope boundary (Unit=Sv). DW import is negligible and net transport is actually equal to the export, import and export were therefore not plotted for the sake of clarity. (c) Cumulated volumes of DW formed at the surface (*Surf*, blue), stored (*V*, green), transported (*Trans*, black) and mixed (*Mix*, red) (Unit= km^3). A positive, resp. negative, value for *Surf*, *Trans* and *Mix* corresponds to production, resp. consumption. (d) Bottom down-slope current (Unit= $\text{m} \cdot \text{s}^{-1}$) and (e) bottom density (Unit= $\text{kg} \cdot \text{m}^{-3}$) at the intersection of the SDS boundary and the Cap Creus canyon.

the shelf, and this further increases the consumption by mixing.

Surf at the end of the DW formation period is similar for W3 and C3, however all the DW is consumed by mixing during W3 while a large part of the DW is stored then exported during C3 (Fig. 9.4c). The surrounding water density difference still explains this difference. Indeed, the heat loss in December is stronger for C3 than for W3 (Fig. 9.4a), the water density over the shelf is therefore higher at the beginning of January (not shown), when surface formation begins. DW export is therefore not only related to the amount of DW formed, but also to the structure of the water column, which also depends on the atmospheric conditions.

9.3.3 Export of dense water

Export of DW from the shelf occurs only between mid-January and end of March (Fig. 9.4b). It does not occur continuously during this period, but shows a strong episodic nature, with flows of DW crossing the shelf-slope boundary, in agreement with observations [Béthoux *et al.*, 2002a; Ivanov *et al.*, 2004]. As for the DW formation, export of DW is highly correlated with the atmospheric heat loss, with a 0.85 correlation factor between HL_{DJFM} and the total quantity of DW exported during the year, $Trans_{TOT}$.

Previous observations [Béthoux *et al.*, 2002a; Canals *et al.*, 2007] and numerical studies [Estournel *et al.*, 2003; Dufau-Julliand *et al.*, 2004; Ulses *et al.*, 2008] showed that due to gravity currents but also to the cyclonic circulation induced by the northwesterly winds, DW formed over the shelf flows southward on the shelf along the coast and escapes the Gulf of Lions shelf at its south-western end. There, due to the narrowing of the shelf, a part of this water escapes it by cascading down the canyons, mainly down the Cap Creus and the Lacaze-Duthiers canyons. The remaining part continues on the shelf along the Spanish coast. The model reproduces correctly these observations, as seen on Fig. 9.5 where the bottom density and current during a strong cascading event in Cap Creus Canyon during year C2 are presented (25th February of year C2, see Fig. 9.4e where the density at the intersection of the Cap Creus canyon and the SDS boundary is shown). We therefore examine the location of DW export : when does DW leave the shelf following the coast, and when does it cascade into the deep ocean ? The SDS boundary is divided in four parts (see Fig. 9.2) : the southwestern end (SW), the Cap Creus canyon (CC), the Lacaze-Duthiers canyon (LC) and the remaining part, the northeastern end (NE). For each year the total quantities of water that escapes the shelf across the whole boundary and across the different parts of the boundary are computed, as well as the mean depth associated to each export. The integrated export as a function of depth is also computed for each year. Results are presented on Fig. 9.6.

For the average and warm years (A1, W1, W2, W3), the small quantity of DW ($< 30 \text{ km}^3$) crossing the boundary escapes the shelf at the SW end (Fig. 9.6a) and in the surface layer, above 200m depth (Fig. 9.6b). On the contrary, during cold years (resp. C1, C2, and C3), resp. 390 km^3 , 810 km^3 and 270 km^3 of DW cross the boundary below 200 m, cascading into the deep ocean (Fig. 9.6b). This cascading represents resp. 53%, 59% and 52% of the total export, and most of this deep export occurs through the Cap Creus Canyon (Fig. 9.6a). In the following, the DW export is defined as the volume of DW flowing across the whole SDS boundary, whereas cascading is defined as the volume of DW flowing across this boundary below 200 m depth.

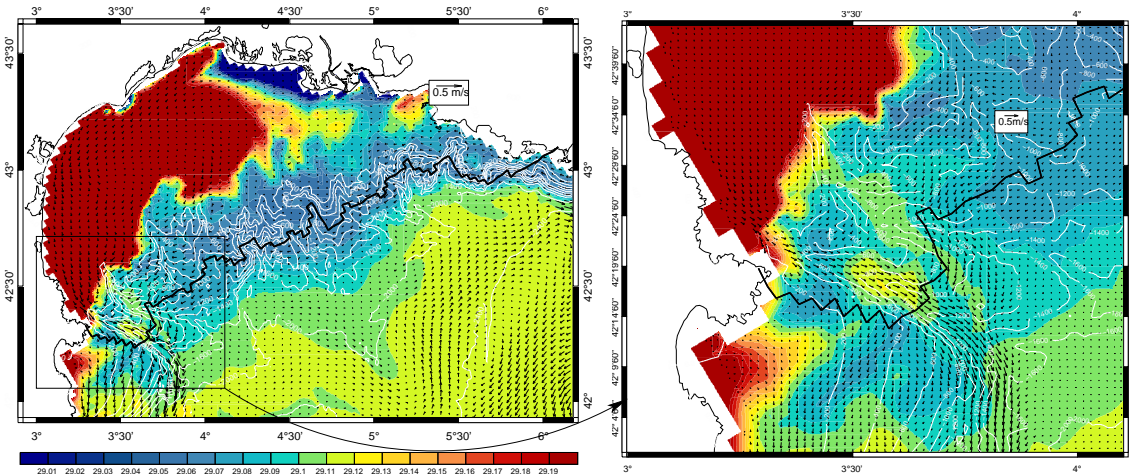


FIG. 9.5 – Cascading event on 25th February of year C2 of the present period ($\rho_{crit} = 29.105 \text{ kg.m}^{-3}$). Bottom density (kg.m^{-3} , map) and current (m.s^{-1} , arrows). White lines : topography. Black line : SDS boundary.

Examining the fate of DW formed at the surface for seven years selected over the present period, we show that the quantity of DW formed over, exported from and cascading from the Gulf of Lions shelf shows a strong interannual variability, which is strongly correlated with the atmospheric conditions, namely with the mean heat loss over the NWMS during the December-March period. Export and cascading are negligible during years with weak heat losses, and all the DW formed at the surface is consumed by mixing. On the contrary, during years with strong heat losses, most of the DW formed at the surface is exported (between 60% and 85%). 50% to 60% of this exported water sinks into the deep ocean, mainly by cascading through the Cap Creus Canyon. There is a threshold effect in the export and cascading of DW, that do not increase linearly with the DW surface formation but occur only if the winter heat loss is larger than the average value.

9.3.4 Comparison with available data

Béthoux et al. [2002a] evaluated that $\sim 440 \text{ km}^3$ of DW cascaded down the slope during winter 1998-99, and *Canals et al.* [2007] estimated that in 2004-2005 $\sim 750 \text{ km}^3$ of DW sank into the deep ocean by cascading down the Cap Creus canyon. Both winters are considered as particularly cold and windy in the NWMS. In our study, for cold years C1, C2 and C3, respectively 390 km^3 , 810 km^3 and 270 km^3 of DW cascades into the deep ocean. These values are of the same order as the observed values. *Palanques et al.* [2006] observed that DW cascading was more intense in the western part of the shelf, and that sediment fluxes during cascading event down the Cap Creus canyon were one to two order of magnitude higher than in the other canyons. Our results are in agreement with those observations : we observe almost no DW export through the NE part of the SDS boundary, and cascading in the Cap Creus canyon represents more than 80% of the deep export during cold years (Fig. 9.6a).

The density contrast corresponds to the difference between the density of the DW formed over the shelf and the density of the ambient surrounding water. For win-

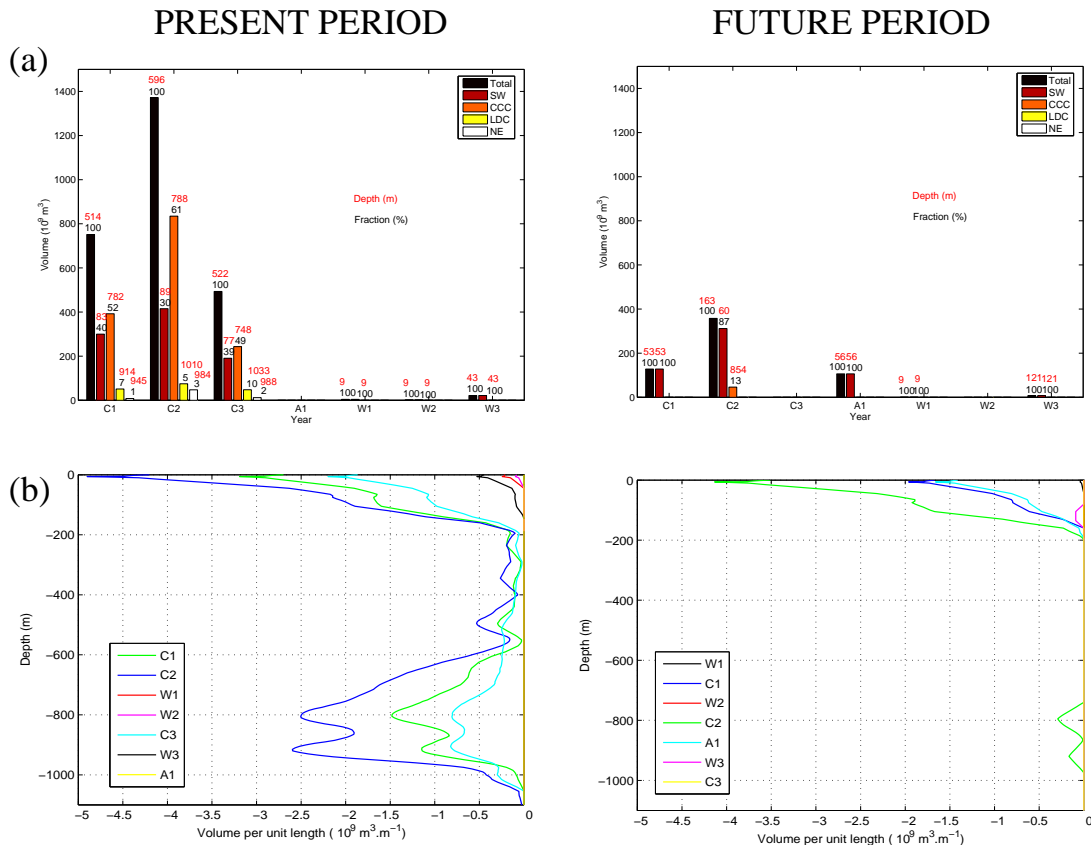


FIG. 9.6 – Export of DW across the SDS boundary during the present and future periods. (a) : export of water through each portion of the SDS boundary (see Fig. 9.2). For each year, the fraction of water exported through each part of the shelf-slope boundary is indicated in black, and the associated depth is indicated in red. (b) : Integrated export as a function of depth

ter 2004-2005, *Canals et al.* [2007] observed a $\sim 0.2 \text{ kg.m}^{-3}$ density contrast. *Ivanov et al.* [2004] report an average density contrast equal to $0.20 \pm 0.25 \text{ kg.m}^{-3}$ for the cascades observed in mid-latitudes regions. For the years selected during the present period and with significant DW cascading (C1, C2, C3), we obtain a difference of density of $\sim 0.30 \pm 0.02 \text{ kg.m}^{-3}$ between the DW present over the shelf and the lighter surrounding water, in good agreement with those observations.

Béthoux et al. [2002a] observed down-canyon currents up to 60 cm.s^{-1} in Lacaze-Duthiers canyon during winter 1998-99 cascading events. *Canals et al.* [2007] recorded current speeds up to 80 cm.s^{-1} in Cap Creus canyon during winter 2004-2005 cascading events. Our model reproduces correctly these current observations : during the modeled cascading events, i.e. when DW bursts occur, we obtain currents varying between 20 and 50 cm.s^{-1} in the Cap Creus canyon (Fig. 9.4d).

For the years of the present period, the observed characteristics of DW cascading (geographical characteristics, current speed, density contrast and DW volume) are correctly represented in the numerical simulations. The modeling strategy used in this study appears to simulate correctly DW formation over and export from the Gulf of Lions continental shelf under present-day climate conditions. It seems therefore legitimate to apply the same strategy to the future period in order to investigate the possible impact of climate change on this process.

9.4 Impact of climate change

In the present section, the effects of climate change on DW formation over and export from the Gulf of Lions shelf are investigated. For that, the amount of water formed at the surface *Surf*, stored *V*, formed by transport *Trans* and formed by mixing *Mix* are computed for each selected year of the future period as was done in Section 9.3 for the present period. Results are presented on Fig. 9.7. Surface formation occurs during the same season as for the present period, i.e. between end of December and beginning of April (Fig. 9.7b). The quantity of water formed at the surface and exported from the shelf still shows an important interannual variability, related to the variability of the atmospheric conditions : DW surface formation still occurs during strong heat loss periods (Fig. 9.7a,b). The temporal behavior of the DW formation is therefore similar to the behavior observed for the selected years of the present period.

The main difference between the present and future periods lies in the volumes of DW formed, exported and cascading. First, the quantity of DW formed at the surface is reduced in average by a factor of 3 between the present and the future periods (Fig. 9.4c and 9.7c). Moreover, for the years with significant DW formation in the future period (C1, C2, A1), the percentage of formed water that escapes the shelf (15% to 50%) is smaller than for the three years of significant export during the present period (C1, C2, C3, 60% to 85%) (Fig. 9.7c and 9.6a). The average exported quantity for C1, C2, A1 in the future period is 4.5 times smaller than for C1, C2, C3 in the present period. Eventually, there is only one year in the future period with DW export into the deep ocean (C2), and this deep export involves a quantity one order of magnitude smaller than volumes cascading during cold years of the present

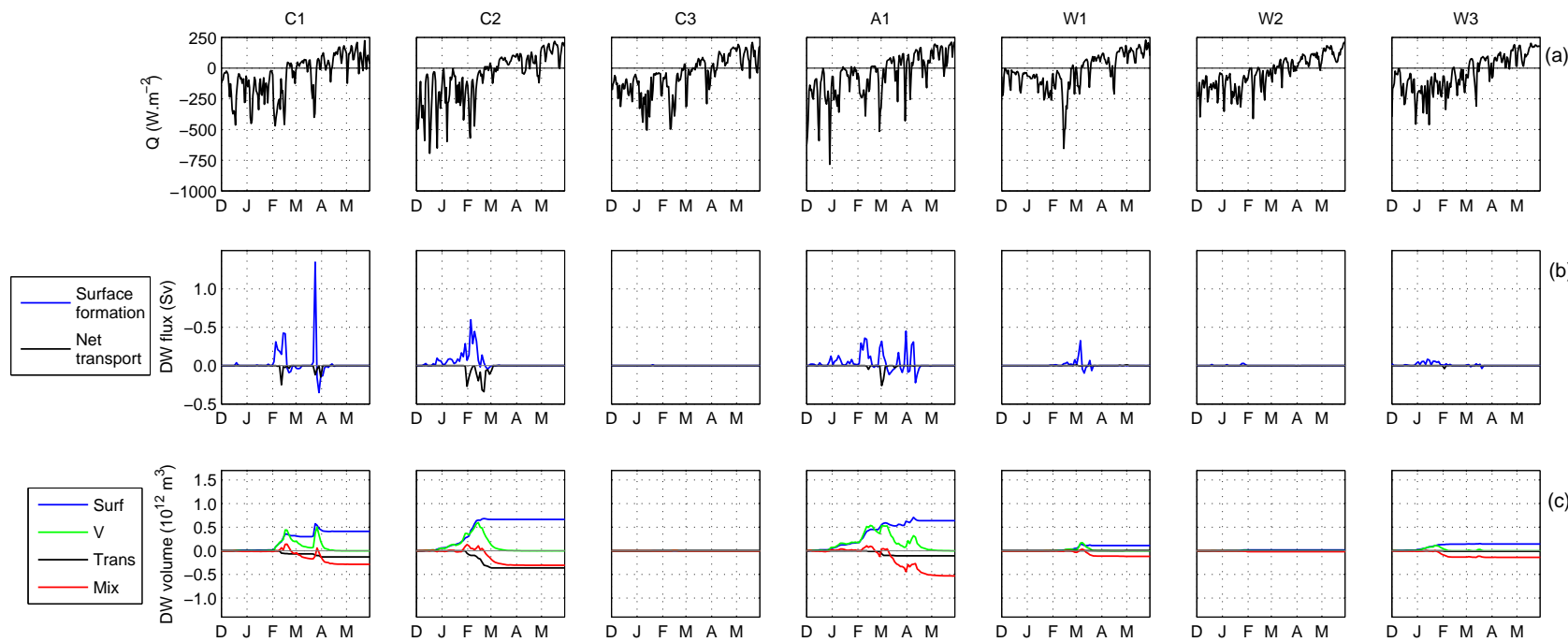


FIG. 9.7 – Evolution of water over the Gulf of Lions shelf during the selected years of the future period. (a),(b),(c) : as for Fig. 9.4

period (Fig. 9.6).

As seen in Section 9.2.1 the heat loss during the winter period, HL_{DJF} , averaged over the whole future and present periods is stronger ($+15 \text{ W.m}^{-2}$) for the future period than for the present period. This is also the case for the heat loss during the DW formation period (December-March) for the selected years. This is shown on Fig. 9.8 where we present the total quantity of DW formed at the surface, $Surf_{TOT}$, vs. the mean heat loss between December and March, HL_{DJFM} . The decrease of volumes of DW formed, exported and cascading can therefore not be attributed to a weakening of the winter heat loss between the 20th century and the end of the 21st century.

In the 140-year simulation performed by *Somot et al.* [2006], the annual mean buoyancy loss decreases in the NWMS during the 21st century ($-2.9 \cdot 10^{-9} \text{ m}^2.\text{s}^{-3}$), resulting in the decrease of the surface density (-0.45 kg.m^{-3}). This density decrease is not homogeneous throughout the water column, and is more important at the surface. The vertical density gradient in the Gulf of Lions is consequently larger at the end of the 21st century than during the 20th century. Computing the mean vertical density gradient along the shelf-slope boundary on 20th December, before the DW surface formation, we indeed obtain a $6.10^{-4} \text{ kg.m}^{-4}$ density gradient averaged over the selected years of the present period vs. a $8.10^{-4} \text{ kg.m}^{-4}$ average density gradient for the future period. This has two consequences.

First, because of this larger density gradient between the surface and 1000m depth, it is more difficult for the surface water to reach the DW criteria (corresponding to the density of the water present in December at 1000m along the SDS boundary) in the future period than in the present period, and a larger buoyancy loss is necessary to produce DW at the surface. The total buoyancy loss BL required to bring the density of the water present over the shelf (corresponding here to the area delimited by the coastline and the SDS boundary, see Fig. 9.2), before the DW formation (i.e. in December) up to the density criteria ρ_{crit} , is

$$BL = \frac{g(\rho_{crit} - \rho_{GDL,S})}{\rho_0} \times D_{GDL} \quad (9.4)$$

where $D_{GDL} \sim 190 \text{ m}$ is the mean depth over this area and $\rho_{GDL,S}$ is the density of the water present over this area, considered as being approximately equal to the surface density. For the atmospheric fluxes used for the ORCM and the SYMPHONIE simulations, for the present period, resp. future period, the heat flux contributes to 87%, resp. 86%, of the buoyancy flux over the Gulf of Lions shelf between December and March, i.e. during the DW formation period. BL is therefore mainly provided by the heat loss. Using equation (9.3), we compute the total heat loss necessary to increase the shelf water density in December up to the density criteria $HL \sim \frac{\rho_0 C_p}{g \alpha BL}$. Dividing HL by the number of seconds in the DJFM period, we obtain the corresponding average heat loss HL_{strat} , in W.m^{-2} , during the surface formation period. As shown in Section 9.3, the variability of the density of the water present over the shelf is more than one order of magnitude higher than the variability of the DW criteria among the selected years, and this is also true for the future period (Table 9.1). We therefore consider the DW criteria as being constant, equal to the average of this criteria for each period (i.e. $\sim 29.1 \text{ kg.m}^{-3}$, resp. $\sim 29.0 \text{ kg.m}^{-3}$, in the present, resp. future period). The surface density obtained in the NWMS in the

ORCM simulation performed by *Somot et al.* [2006], that provides the boundary conditions for the regional model, is used to compute the average of this heat loss over the 30-year present and future periods, $HL_{strat,p}$ and $HL_{strat,f}$: $HL_{strat,p}=216.9 \text{ W.m}^{-2}$ and $HL_{strat,f}=246.1 \text{ W.m}^{-2}$. The 29.2 W.m^{-2} difference between $HL_{strat,f}$ and $HL_{strat,p}$ corresponds to the additional heat loss required to increase the shelf water density up to the DW criteria in the future period compared to the present period, due to the stronger stratification. This additional heat loss explains that the quantity of DW formed in the future is much smaller than in the present, for an equivalent atmospheric heat loss, as observed on Fig. 9.8. The 15 W.m^{-2} average winter heat loss increase between the 20th and 21st centuries, twice smaller than the additional heat loss, is not sufficient to counterbalance it. As explained in Section 9.3.2, this reduction of the volume of DW formed favors the mixing consumption. Second, during the DW formation period, DW is surrounded on the shelf with water whose density difference compared with water present at 1000m depth before the formation period is larger in the future period than in the present period because of the stronger stratification. The difference between DW and this surrounding water is indeed $\sim 0.35 \pm 0.06 \text{ kg.m}^{-3}$ in the present vs. $\sim 0.49 \pm 0.11 \text{ kg.m}^{-3}$ in the future (we do not take into account the two years with practically no surface formation, C3 and W2, in the future period). When DW formed at the surface is mixed with the surrounding water, the resulting water density decreases more in the future period than in the present period.

The stronger vertical density gradient, by reducing the amount of DW formed and the density of the surrounding water, therefore explains that DW is mainly consumed by mixing in the future period, even for the coldest years (Fig. 9.7c), and that less water is available for export. Furthermore, since the difference between the density of the DW that reaches the SDS boundary and the DW criteria is smaller than for the present period, the DW can less easily cascade into the deep ocean, as observed on Fig. 9.3 : cascading water density is higher than the density of the water present at 2000m depth in the present period, whereas it is comparable with the density of water present between 1100m and 1300m in the future period. As a result, because of the larger mixing consumption due to the stronger stratification, the fraction of exported water that sinks into the deep ocean is much smaller in the future period than in the present period (Fig. 9.6) : there is only one year (C2) with significant deep export, representing only 8% ($\sim 30 \text{ km}^3$) of the total export ($\sim 360 \text{ km}^3$), 92% of the water being exported in the surface layer. In the present period, for the selected years with significant water export, deep export represents between 50% and 60% of DW export, with volumes varying between 270 km^3 and 810 km^3 , one order of magnitude higher.

For the selected years of the future period, the change in the water column structure induced by the decrease of annual surface buoyancy loss during the 21st century explains that, at equivalent winter surface heat loss, less DW is formed at the surface in the future period, a smaller fraction of this DW is exported, and an even smaller fraction sinks into the deep ocean, compared with years of the present period. For these selected years, cascading practically disappears in the future, being reduced at least by $\sim 90\%$. The results obtained for the selected years of each period are extrapolated to the whole 30-years periods in the next section.

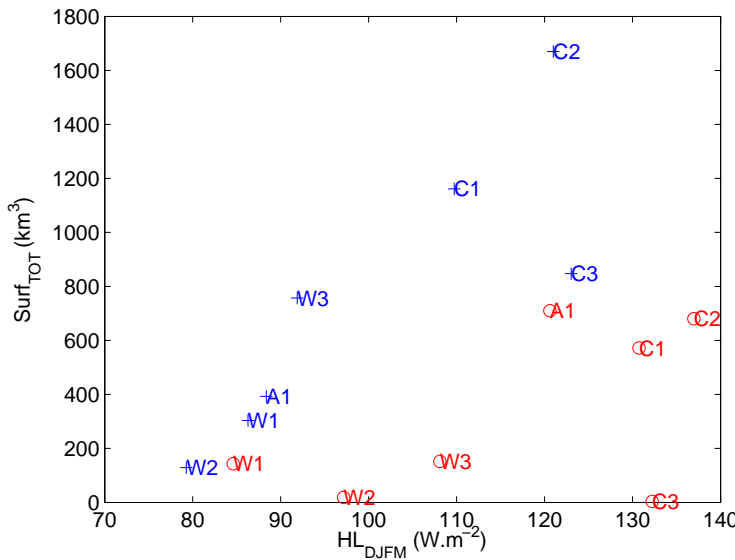


FIG. 9.8 – Dense water formed at the surface ($Surf_{TOT}$, km^3) vs. heat loss between December and January (HL_{DJFM} , $\text{W} \cdot \text{m}^{-2}$). Blue crosses, resp. red circles : selected years of the present, resp. future period.

9.5 Extrapolation to the whole present and future periods

It was shown in Section 9.3 that DW formation, export and cascading over the Gulf of Lions shelf show a high interannual variability, which is strongly correlated with the atmospheric winter heat loss over the NWMS, HL_{DJFM} (correlation factors=0.85, 0.85 and 0.83). These correlations are used to extrapolate our results to the whole 30-year present and future periods.

Fig. 9.8 shows that for equivalent atmospheric heat loss, DW surface formation in the future period is much smaller than in the present period. As explained in Section 9.4, this is due to the stronger stratification of the water column in the Gulf of Lions before the DW formation period. Surface formation is therefore not related only to the atmospheric heat loss, and the initial stratification of the water column must be taken into account. Instead of relating simply the quantity of DW formed at the surface, $Surf_{TOT}$, with the December-March atmospheric heat loss, HL_{DJFM} , it is more meaningful to relate $Surf_{TOT}$ with the difference between the atmospheric heat loss and the heat loss necessary to bring the shelf water density up to the density criteria, $HL_{DJFM} - HL_{strat}$. HL_{strat} indeed represents the heat loss necessary to bring the shelf water up to the criteria, and this difference can be considered as the “effective” heat loss HL_{eff} , i.e. the heat loss responsible for DW formation. The values of HL_{strat} computed in Section 9.4, $HL_{strat,p}$ and $HL_{strat,f}$, are used in the following analysis. $Surf_{TOT}$ is plotted vs. $HL_{DJFM} - HL_{strat} = HL_{eff}$ on Fig. 9.9a. The relationship between the DW formed quantity and the “effective” heat loss seems to be the same for the present and future periods. A linear regression analysis of the form $y = ax + b$ between $y = Surf_{TOT}$ and $x = HL_{eff}$ is performed. The corresponding fit, resulting in a 13.8% relative error, is shown on Fig. 9.9a. The

relative error is given by

$$\epsilon = \frac{1}{14} \sum_{SEL} \frac{|Surf_{TOT,predicted} - Surf_{TOT,model}|}{\max_{SEL} (Surf_{TOT,model})} \quad (9.5)$$

where $Surf_{TOT,predicted}$ is the quantity of water formed at the surface during each year using the linear equation, $Surf_{TOT,model}$ is the quantity predicted by the model, and SEL is the ensemble of the 14 selected years. The obtained regression is then used to estimate the surface formation volume for each year of the present and future periods : $Surf_{TOT} = \max(0, a \times HL_{eff} + b)$ (see Fig. 9.9a (dots) and Fig. 9.10). Taking the average of this value over the whole period, the mean annual surface formation volume for the present period is 788 km^3 with a 421 km^3 standard deviation, and 397 km^3 with a 312 km^3 standard deviation for the future period. For both periods the interannual variability is high, of the same order as the average value. In average, the quantity of DW formed at the surface is divided by 2 between the 20th century and the end of the 21st century, due to the strengthening of the stratification. For the present period, we obtain one year, out of 29, with a zero-surface formation, vs. 5 for the future period.

A relation $y = f(x)$ between $x = HL_{eff}$ and the total net exported quantity of DW, $y = Trans_{TOT}$, is then established. It was observed in Section 9.3 that $Trans_{TOT}$ was negligible for the warm and average years (for which $HL_{DJFM} \leq \overline{HL}_{DJFM,p}$, where the overbar denotes the average over the 30 years), corresponding to a threshold effect of the winter heat loss. Following this observation, we consequently assume empirically that export is possible only if the effective heat loss is larger than the average effective heat loss over the 30 years of the present period : $HL_{eff} \geq \overline{HL}_{eff,p}$, equivalent to $HL_{DJFM} \geq \overline{HL}_{DJFM,p}$ for the present period. This implies that $f(x)$ verifies

$$\begin{cases} f(x) = 0 & \text{for } x < HL_{eff,min} \\ f(x) = ax + b & \text{for } x \geq HL_{eff,min} \end{cases} \quad (9.6)$$

for both periods, where $HL_{eff,min} \geq \overline{HL}_{eff,p}$ is the minimum effective heat loss for which export begins. The continuity of $f(x)$ at $x = HL_{eff,min}$ provides $b = -a \times HL_{eff,min}$. We performed a linear regression analysis of the form $y = ax'$ between $x' = x - HL_{eff,min}$ and $y = Trans_{TOT}$, varying $HL_{eff,min}$ in $[\overline{HL}_{eff,p} = -110 \text{ W.m}^{-2}, -80 \text{ W.m}^{-2}]$ and using only the selected years verifying $HL_{eff} > \overline{HL}_{eff,p}$, i.e. years C1, C2, C3 of the present period and year C2 of the future period. The same method is used to obtain a relation between $x = HL_{eff}$ and $y = Casc_{TOT}$. The corresponding fit, resulting in a 11%, resp. 8%, relative error for $Trans_{TOT}$, resp. $Casc_{TOT}$, is shown on Fig. 9.9b, resp. 9.9c. The minimum relative error is obtained in both cases for $HL_{eff,min} = \overline{HL}_{eff,p}$: export and cascading begin when $HL_{eff} = \overline{HL}_{eff,p}$. Taking the average of the predicted value over the whole period, the mean annual DW export for the present period is 597 km^3 with a 870 km^3 standard deviation, and 62 km^3 with a 250 km^3 standard deviation for the future period. The mean annual DW cascading is 335 km^3 with a 489 km^3 standard deviation for the present period, and 36 km^3 with a 140 km^3 standard deviation for the future period. Interannual variability is strong for each period. Between the 20th century and the end of the 21st century, DW export and cascading decrease in average by 90%. When considering only years with significant export and cascading, defined

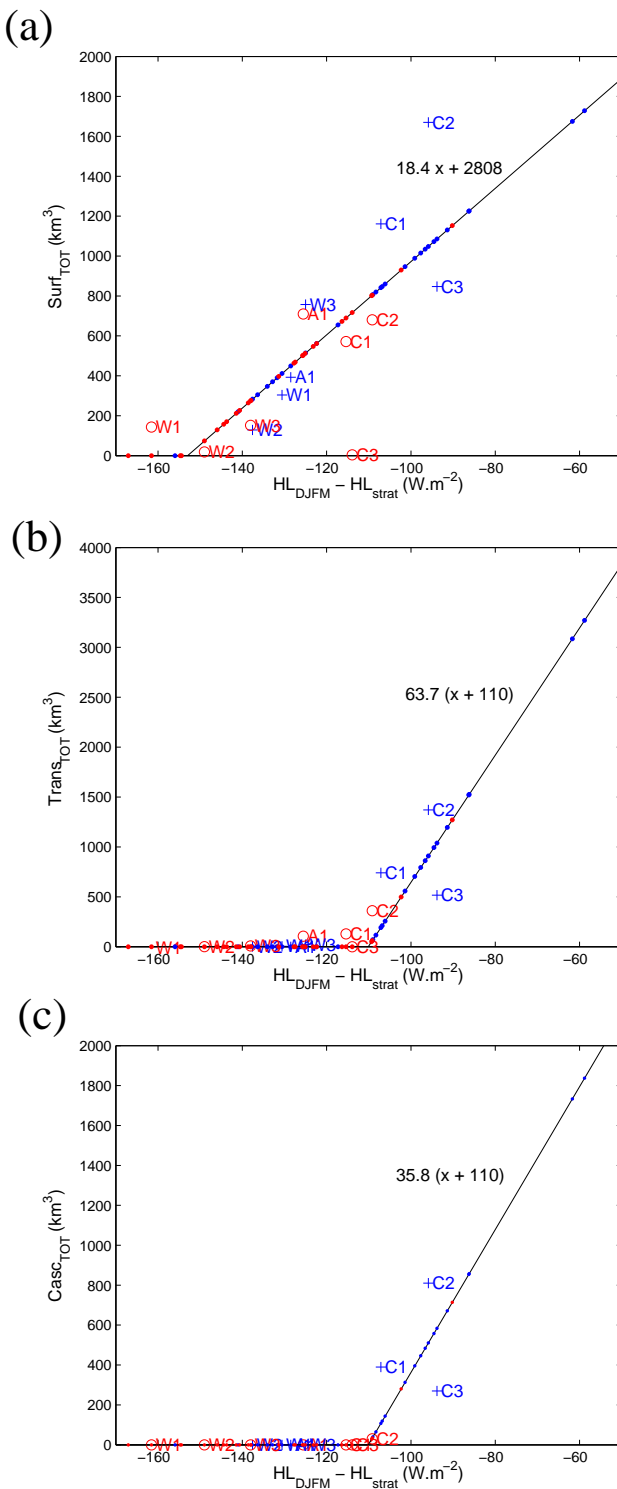


FIG. 9.9 – DW formed, exported and cascading for the present (blue) and future (red) periods. (a) : Total DW volume formed at the surface during a given year, $Surf_{TOT}$, as a function of the difference between the mean heat loss during the formation period for this given year and the mean heat loss corresponding to the stratification, $HL_{DJFM} - HL_{strat}$. (b) and (c) : same for exported water $Trans_{TOT}$ and cascading water $Casc_{TOT}$. + and o : selected years for the present and future periods. • : results obtained for each year of the present and future period using the obtained regression. Black line : linear regression analysis.

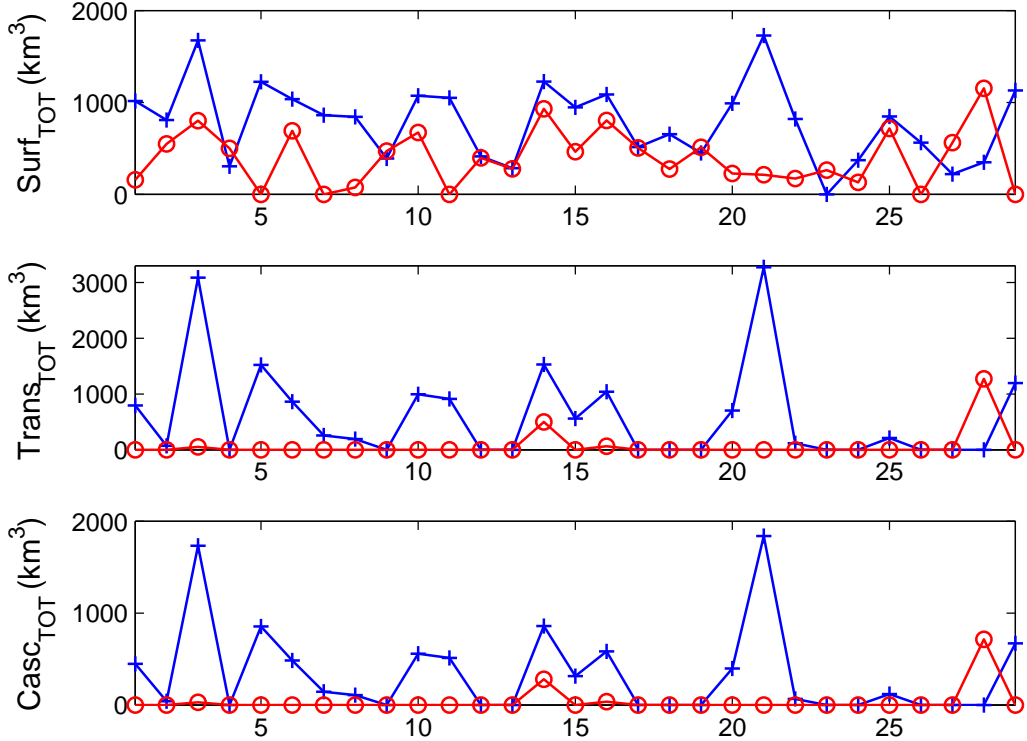


FIG. 9.10 – DW formed, exported and cascading for each year of the present (blue, \circ) and future (red, $+$) periods.

as years with exported and cascading volumes larger than 100 km^3 , one obtains 15 years for the present period, with average export and cascading of 1140 km^3 and 640 km^3 , and 2 for the future period, with average values of 1018 km^3 and 570 km^3 (Fig. 9.10). This means that the decrease of the mean annual export and cascading is mainly due to the decrease of the number of years with export and cascading : significant volumes, of the same order as under present climate conditions can still be exported and cascade at the end of the 21st century, but exceptionally, requiring exceptionally cold winter atmospheric conditions to compensate the stronger stratification.

The 90% mean decrease is almost twice stronger than the surface formation decrease. As explained in Section 9.4, in the future period, DW is indeed mainly eliminated by mixing because of the stronger stratification : as a result, 75% of the water formed at the surface is exported in the present period, vs. 16% in the future period.

For the years with the strongest heat losses, export can be higher than surface formation (e.g. years 2 and 21 of the present period, Fig. 9.10) : this is due to the fact that the two curves ($Surf_{TOT}$ vs. HL_{eff} and $Trans_{TOT}$ vs. HL_{eff}) cross each other for high values of the heat loss (Fig. 9.9). Physically, this corresponds to the fact that the heat loss is so high that the mixing of the DW formed at the surface with lighter surrounding water produces DW, as observed for some of the selected years in Section 9.3, resulting in a significant increase of the quantity of DW present over the shelf and then exported.

9.6 Uncertainties

In the previous sections, numerical simulations performed with the regional oceanic model SYMPHONIE, forced at its lateral boundary by the ORCM OPA and at the surface by the ARCM ARPEGE-Climate under the IPCC A2 scenario forcings, were used to investigate the impact of interannual atmospheric variability and climate change on the quantities of DW formed over, exported from and cascading from the Gulf of Lions shelf. Respectively 50%, 90% and 90% decreases between the 20th century and the end of the 21st century were estimated for the average yearly volume of DW formed, exported and cascading. In this section, we provide an estimate of the uncertainties associated to the choice of the DW criteria, the parameters of the regional oceanic model, the water flux, the choice of the atmospheric model and the choice of the IPCC scenario.

9.6.1 Sensitivity test to the dense water criteria

In Section 9.2.3 the DW density criteria was defined as $\rho_{crit} = \rho_{bottom} + \Delta\rho$, where ρ_{bottom} is the mean density at the bottom of the boundary during the month preceding cascading, i.e. December, and $\Delta\rho = 0.03 \text{ kg.m}^{-3}$ is a constant density anomaly. Sensitivity tests to this criteria are performed here by varying $\Delta\rho$. Fig. 9.3 shows that the DW patch could also be defined using $\Delta\rho = 0.02 \text{ kg.m}^{-3}$ instead of $\Delta\rho = 0.03 \text{ kg.m}^{-3}$, we therefore vary $\Delta\rho$ between 0.02 and 0.04 kg.m^{-3} .

The impact of the density criteria choice on the absolute quantities is first examined for the present period. The mean and standard deviation over the selected years of the present period of the relative difference between volumes obtained using $\Delta\rho \in [0.02, 0.025, 0.035, 0.040] \text{ kg.m}^{-3}$ and volumes obtained using $\Delta\rho = 0.03 \text{ kg.m}^{-3}$, $\frac{|value_{year,\Delta\rho} - value_{year,0.03}|}{value_{year,0.03}}$, are given in Table 9.2. The impact of $\Delta\rho$ on the amount of DW formed at the surface is much weaker than the impact on the volumes of exported and cascading DW, which vary by a factor of 2. The density of the DW formed at the surface is indeed much larger than the criteria (see for example Figure 9.5), explaining that the impact of the criteria on the quantity of DW formed is relatively weak. On the contrary, since the originally very dense water formed at the surface was mixed with lighter water during its way to the boundary, the density of the exported and cascading water is closer to the criteria. The volume of exported and cascading DW therefore depends a lot on the choice of the criteria. Note however that values of $\Delta\rho \geq 0.03 \text{ kg.m}^{-3}$ give more realistic values for the cascading volumes than values of $\Delta\rho < 0.03 \text{ kg.m}^{-3}$, which give results that are in the highest range of the observations (see Section 9.3.4).

Since the objectives of the present study are to investigate first the impact of atmospheric interannual variability on DW formation, export and cascading under present climate conditions, and second the impact of climate change, we are particularly interested in the relative values between the years and the periods. We compute for each value of $\Delta\rho$ the difference between volumes obtained for each selected year of each period and for the year with the highest volumes, which is always year C2 of the present period, $\frac{|value_{year,\Delta\rho} - value_{C2,\Delta\rho}|}{value_{C2,\Delta\rho}}$. Results are presented in Table 9.3 for the present period and in Table 9.4 for the future period. For the formation, the export and the cascading and for each year of the future and present periods, the much smaller values of the standard deviation compared to the average value of

TAB. 9.2 – Mean and standard deviation (bracket) over the selected years of the present period of the relative difference between the total volume of DW formed at the surface (*Surf*), exported (*Trans*), and cascading (*Casc*) obtained for different values of $\Delta\rho$ and the volume obtained for $\Delta\rho = 0.03 \text{ kg.m}^{-3}$, $\frac{|value_{year,\Delta\rho} - value_{year,0.03}|}{value_{year,0.03}}$. Values for cascading are computed using results for years with significant cascading, i.e. C1, C2, C3.

$\Delta\rho$	0.02	0.025	0.035	0.04
<i>Surf</i>	0.18 (0.19)	0.10 (0.12)	0.11 (0.09)	0.17 (0.09)
<i>Trans</i>	0.44 (0.44)	0.29 (0.35)	0.12 (0.12)	0.25 (0.17)
<i>Casc</i>	1.32 (0.63)	0.53 (0.30)	0.28 (0.07)	0.47 (0.08)

the relative difference show that the choice of the DW criteria does not have a significant impact on the relative difference between the years and the periods. Our conclusions concerning the relative impacts of atmospheric interannual variability and climate change on DW formation, export and cascading on the Gulf of Lions shelf are independent on the DW criteria.

9.6.2 Sensitivity to the parameters of the regional oceanic model

The parameters used in the high-resolution model can induce uncertainty in the results. The fate of the DW formed over the shelf could be particularly dependant on the horizontal diffusivity and on the bottom friction. Given the wide range of variability obtained, an error on a large amount of water formed or transported will have a much larger impact on the variability of the averaged results for each period than an error on a small amount of water. Therefore, we tested the sensitivity to the different parameters by performing additional simulations for the most productive year of the present period, year C2.

The horizontal diffusivity

In SYMPHONIE, a classic centered advection scheme is used for the velocity [Arakawa and Suarez, 1983], with the horizontal viscosity $K_H = 60 \text{ m}^2.\text{s}^{-1}$. There is no explicit horizontal viscosity for the tracers, since it is implicitly included in

TAB. 9.3 – Mean and standard deviation (bracket) over the selected years of the present period of the relative difference between the total volume of DW formed at the surface (*Surf*), exported (*Trans*), and cascading (*Casc*) obtained during years of the present period and year C2, $\frac{|value_{year,\Delta\rho} - value_{C2,\Delta\rho}|}{value_{C2,\Delta\rho}}$, for different values of $\Delta\rho$.

Year	C1	C3	A1	W1	W2	W3
<i>Surf</i>	0.50 (0.05)	0.45 (0.04)	0.21 (0.02)	0.16 (0.02)	0.06 (0.01)	0.40 (0.03)
<i>Trans</i>	0.57 (0.05)	0.44 (0.05)	0 (0)	0 (0)	0 (0)	0.02 (0)
<i>Casc</i>	0.51 (0.03)	0.44 (0.08)	0 (0)	0 (0)	0 (0)	0 (0)

TAB. 9.4 – Mean and standard deviation (bracket) over the selected years of the future period of the relative difference between the total volume of DW formed at the surface (*Surf*), exported (*Trans*), and cascading (*Casc*) obtained during years of the future period and year C2 of the present period, $\frac{|value_{year,\Delta\rho} - value_{C2,\Delta\rho}|}{value_{C2,\Delta\rho}}$, for different values of $\Delta\rho$.

Year	C1	C2	C3	A1	W1	W2	W3
<i>Surf</i>	0.25 (0.02)	0.36 (0.07)	0 (0)	0.40 (0.02)	0.07 (0.02)	0.01 (0)	0.08 (0.01)
<i>Trans</i>	0.10 (0.04)	0.28 (0.07)	0 (0)	0.08 (0.03)	0 (0)	0 (0)	0 (0)
<i>Casc</i>	0 (0)	0.03 (0.01)	0 (0)	0 (0)	0 (0)	0 (0)	0 (0)

the numerical advection scheme, a hybrid centered/upstream scheme adapted from *Beckers* [1995]. We performed sensitivity tests to the horizontal diffusivity for the velocity K_H multiplying and dividing it by 2 in the simulation for year C2 of the present period. The maximum variation is $\Delta \sim 7\%$ for the annual volume of DW formed at the surface. The annual export ($\Delta \sim 16\%$) and cascading ($\Delta \sim 25\%$) are more sensitive to the horizontal diffusivity. This seems physically logical : the velocity influences the fate of DW when this DW is moving, therefore not when it is formed at the surface, but rather when it is exported.

The bottom friction

The bottom friction should only play a role when the DW flows along the bottom. It should consequently not influence considerably the surface formation, but rather the export and the cascading. It is indeed one of the key factors in the cascading process, as explained by *Simpson* [1987] : large scale geostrophic currents tend to flow along the bathymetric isolines, inhibiting the exchanges between the shelf and the open ocean through the continental slope. The bottom friction and the channeling by the topography counteract this geostrophic tendency, allowing the dense water formed over the shelf to flow down the slope by gravity current. In SYMPHONIE, the bottom friction $\vec{\tau}_b$ is related to the bottom velocity \vec{V}_b (equal in the model to the velocity at the first level above the bottom) by a quadratic relationship :

$$\vec{\tau}_b = \rho_0 C_D \|\vec{V}_b\| \vec{V}_b \quad (9.7)$$

where C_D is the bottom friction coefficient, related to the bottom roughness z_0 by a logarithmic law :

$$C_D = \left(\frac{\kappa}{\log\left(\frac{z_1}{z_0}\right)} \right)^2 \quad (9.8)$$

with $\kappa = 0.41$ the Von Karman constant and z_1 the height of the first level above the bottom. In our model, $z_0 = 1\text{cm}$, following *Blumberg and Mellor* [1987]. This is an upper bound for the bottom roughness. $5 \cdot 10^{-4}\text{m}$ can be considered as a lower bound. This range of values is indeed classically used in sediment transport modelling to take into account the roughness induced by sand, by waves and by bedforms present on the bottom of the sea. We performed a simulation for the year C2 of the present period, with $z_0 = 5 \cdot 10^{-4}\text{m}$. As expected, the sensitivity of the quantity

of water formed at the surface to the bottom friction parametrization is small (the annual surface formation decreases by -4%), but the sensitivity of the export, that decreases by 27% and of the cascading, that decrease of 55%, are more important.

Finally, the annual quantity of DW formed at the surface is not very sensitive to the parameters of the model, and one can estimate the computation error for this volume to be less than 10%. The export and cascading are more sensitive to those parameters, in particular to the bottom friction. An upper bound for the computation error can be estimated from the sensitivity tests made here as $\sim 30\%$ for the export and $\sim 55\%$ for the cascading. The influence of those parameters on the absolute results obtained for each given year is therefore not negligible. However, an error on a given parameter would change the results in the same direction (increase or decrease) for each year. As for the uncertainty due to the dense water criteria, the results concerning the relative differences between different years of the same period or between the present and the future period should therefore not be fundamentally different.

9.6.3 Sensitivity to the water flux

Due to the weaker ability of ARCM to simulate the precipitations, the surface atmospheric water loss term represents a source of uncertainty in our study [Li *et al.*, 2006]. However, the boundary conditions for SYMPHONIE are prescribed using the results of the simulation of Somot *et al.* [2006], who observed that the $(E - P)$ term simulated by their ARCM is in good agreement with the observations. In winter, over the shelf, the atmospheric water flux contribution to the buoyancy flux is one order of magnitude smaller than the heat flux contribution, as seen in section 9.4. For a given winter, an error on the winter atmospheric water flux term should therefore not influence significantly the stratification and the results.

The value of the coefficients used to compute the future period Rhône runoff is another source of uncertainty. For the 10 different ARCMs of the PRUDENCE project (see section 9.6.4), the decrease of the Rhône runoff (see section 9.2.2) between the 20th and the 21st centuries varies between 0 and 20% (Hagemann, personnal communication), 20% being the value obtained in the ARPEGE-Climate simulation [Gibelin and Déqué, 2003] and used here. Considering only the effect of the Rhône river variation, the present studies therefore provides a lower bound for the induced decrease of DW formation, export and cascading. A weaker runoff decrease will indeed contributes more to the enhancement of the stratification.

The runoff variation between the present and the future periods induces an average buoyancy variation over the shelf that is one order of magnitude smaller than the winter atmospheric buoyancy flux. However, contrary to the atmospheric buoyancy flux, the Rhône buoyancy flux is concentrated in one point of the domain, and can locally influence the water column structure. It is therefore more difficult to estimate the effect of a small variation of this source of buoyancy. Performing a simulation for the most productive year of the future period (C2) with no runoff variation compared to the present period, the DW surface formation, export and cascading are respectively 10%, 40%, and 100% smaller than in the simulation with the 20% runoff decrease. For a given winter in the future period, the impact of the Rhône runoff of the surface formation is small. The impact on the export and cascading seems

more spectacular, one should however keep in mind that this impact concerns values that are already very small. Extrapolating those results to the whole period, one can estimate that the uncertainty on the Rhône runoff would cause the DW surface formation, export and cascading decrease between the 20th and 21st centuries to vary respectively between 50 and 55%, 90 and 94% and 90 and 100%.

On the short term, errors on the winter water flux term and on the runoff coefficient would not change significantly the results concerning the impact of climate change. However, on the annual scale, the atmospheric water flux and heat flux contributions are similar ($\sim 50\%$ for the present period). The annual buoyancy gain due to the Rhône runoff is almost twice the average annual atmospheric buoyancy loss. An error on the annual atmospheric water flux or on the river runoff variation could therefore influence significantly the annual buoyancy flux that plays a major role in the evolution of the water column stratification during the 21st century. This would have an impact on the results regarding the formation and fate of DW for the future period. To investigate the sensitivity of our results to long-term variations of the river and atmospheric water fluxes, it would now be necessary to perform other 140-year ORCM simulations.

The impact of the interannual variability of the Rhône river runoff was not investigated in this paper. The winter runoff can vary by a factor of 2 from one year to another. Such a variation represents a variation of buoyancy flux of the same order as the winter atmospheric buoyancy loss. One can then expect the interannual variability of the Rhône river runoff to influence the water column stratification and the DW shelf formation and fate, on the short term as well as on the long term. Further modeling studies should be performed to investigate this effect.

9.6.4 Sensitivity test to the Atmospheric Regional Climate Model (ARCM)

In the present study, the results of a simulation performed with the ARCM ARPEGE-Climate [*Gibelin and Déqué*, 2003], used by *Somot et al.* [2006] to force the ORCM OPA, were used to force the regional model SYMPHONIE at the surface. However, several other atmospheric models are available, for example 10 ARCMs were used to simulate the present-day climate over Europe, as well as the impact of climate change by the end of the 21st century, in the framework of the PRUDENCE project [*Christensen et al.*, 2002]. Each ARCM is forced at its boundaries by an atmosphere-ocean general circulation model (AOGCM). Analysing the results of these simulations for the present period (1961-1990), *Jacob et al.* [2007] showed that the main ARCM systematic biases vary among the models, in particular the bias of the winter air temperature over the land. Winter heat loss can therefore be expected to show a non negligible bias across the different models. *Déqué et al.* [2007] assessed uncertainties in projected climate change, examining uncertainties due to the ARCM, to the forcing AOGCM, and to the natural internal variability due to the chaotic nature of the atmosphere behavior. The objectives of the present section is to assess uncertainties in DW formation and export modeling in the Gulf of Lions shelf due to the choice of the ARCM, the choice of the AOGCM, the natural variability and the choice of the climate change scenario.

For this purpose, climate simulations performed with the eight ARCMs for which data necessary to compute the winter heat loss are available were selected for the

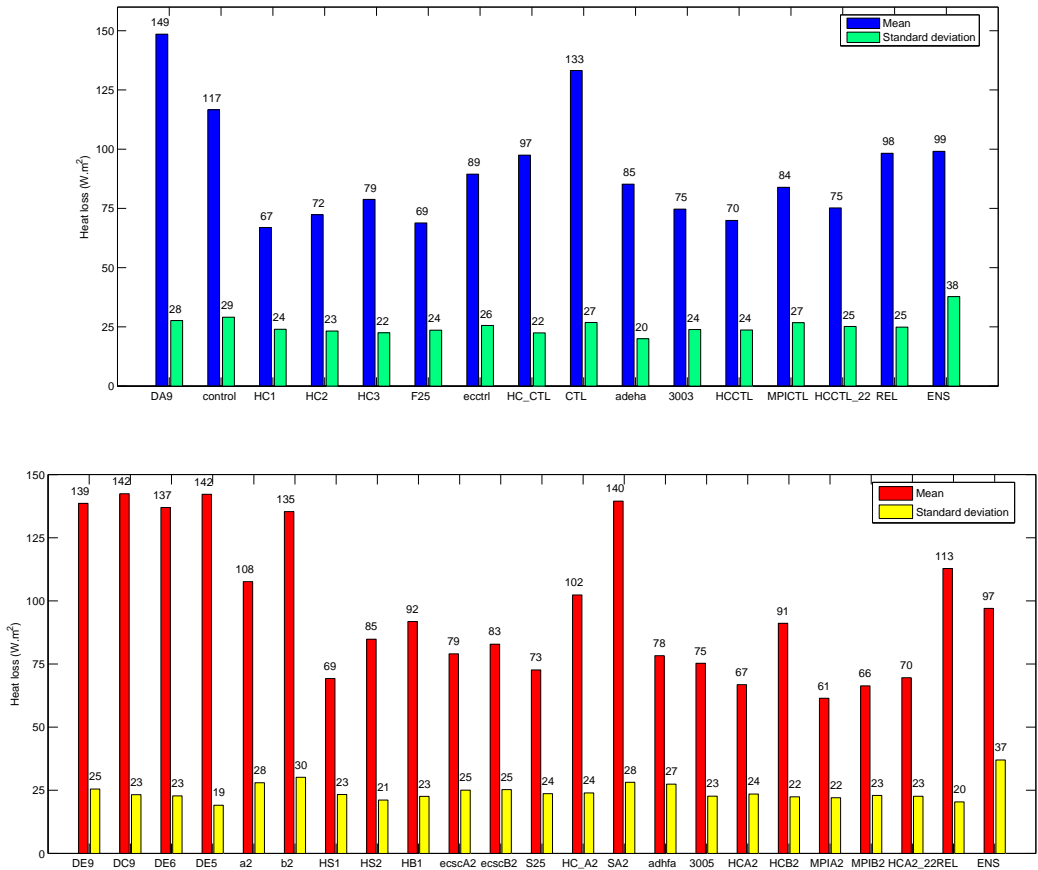


FIG. 9.11 – Average and standard deviation of the mean December–March total heat loss over NWMS, HL_{DJFM} (W.m^{-2}), for each present-day climate simulation (top) and end of the XXIth century simulation (bottom) selected from the PRUDENCE project. REL corresponds to the heat loss of the ARCM ARPEGE-Climate simulations DA9 and DE9 corrected by the relaxation term, used to force the regional model SYMPHONIE (see Section 9.2.1). ENS corresponds to the 240-year ensemble mean formed by the eight present-day climate simulations for the eight ARCM (see Tables 5 and 6).

TAB. 9.5 – List of 1961-1990 simulations used in this study. The eight simulations marked with (*) were used to build the 240-year ensemble mean ENS. ARCM : Regional Climate Model. AOGCM : Atmosphere Ocean Global Climate Model. Res. : spatial resolution

Institute	Run name	ARCM	AOGCM	Res.
CNRM(*)	DA9	ARPEGE	ARPEGE	50 km
UCM(*)	control	PROMES	HadAM3H	50 km
DMI(*)	HC1	HIRHAM	HadAM3H	50 km
DMI	HC2	HIRHAM	HadAM3H	50 km
DMI	HC3	HIRHAM	HadAM3H	50 km
DMI	F25	HIRHAMh	HadAM3H	25 km
DMI	ecctrl	HIRHAM	ECHAM4	50 km
ETH(*)	HCCTL	CHRM	HadAM3H	55 km
GKSS(*)	CTL	CLM	HadAM3H	55 km
HC(*)	adeha	HadRM3P	HadAM3H	50 km
MPI(*)	3003	REMO	HadAM3H	55 km
SMHI(*)	HCCTL	RCAO	HadAM3H	50 km
SMHI	MPICTL	RCAO	ECHAM4	50 km
SMHI	HCCTL22	RCAOh	HadAM3H	22 km

present (1961-1990, 14 simulations) and future (2071-2100, 21 simulations) periods (see Tables 5 and 6). Each of the eight institutes provides a basis simulation for the present and future periods (denoted by * in Tables 5 and 6), and some institutes provide some additional simulations. The DA9 and DE9 simulations are actually the present and future parts of ARCM simulation used to force the ORCM (see Section 9.2.1).

The total heat loss HL is the sum of the net longwave flux radiation LW , the net shortwave radiation SW , the latent heat flux LH and the sensible heat flux SH . Monthly data for LW and SW are directly available on the PRUDENCE project website (prudence.dmi.dk). LH is computed using the monthly evaporation E : $LH = \rho_0 AE$ where $A = 2.47 \cdot 10^6 \text{ J} \cdot \text{kg}^{-1}$ is the latent heat of condensation and $\rho_0 = 1020 \text{ kg} \cdot \text{m}^{-3}$ is the reference sea water density. Daily wind velocity and air temperature data were extracted to compute the sensible heat flux : $SH = \rho_a C_{pa} C_h V_a (SST - T_a)$ where $\rho_a = 1.2 \text{ kg} \cdot \text{m}^{-3}$ is the air density, $C_{pa} = 1004 \text{ J} \cdot \text{kg}^{-1} \cdot \text{K}^{-1}$ is the specific heat of air, $C_h = 1.2 \cdot 10^{-3}$ is the Stanton number, V_a is the 10-metre wind velocity, SST is the sea surface temperature and T_a is the 2-metre air temperature. SST values used in the ORCM simulation (see Section 9.2.1) is used for SST . The mean December-March total heat loss over NWMS, HL_{DJFM} , is obtained for each year of each simulation.

The average and standard deviation of HL_{DJFM} are shown for both periods and for the different simulations on Fig. 9.11. REL is not a real simulation but represents the heat loss obtained when adding the relaxation heat flux to the heat flux of the DA9 and DE9 simulations (see Section 9.2.1). This heat loss is actually the one used to force the regional model SYMPHONIE. For both period, the ensemble mean ENS is the 240-year ensemble of the eight basis simulations of each institute (* in Tables 5 and 6). In agreement with the variability of the temperature observed

TAB. 9.6 – List of 2071-2100 simulations used in this study. The eight simulations marked with (*) were used to build the 240-year ensemble mean ENS. ARCM : Regional Climate Model. AOGCM : Atmosphere Ocean Global Climate Model. Res. : spatial resolution. Sc. : IPCC scenario

Institute	Run name	ARCM	AOGCM	Res.	Sc.
CNRM	DE9	ARPEGE	ARPEGE	50 km	A2
CNRM	DC9	ARPEGE	ARPEGE	50 km	B2
CNRM(*)	DE6	ARPEGE	HadAM3H	50 km	A2
CNRM	DE5	ARPEGE	HadAM3H	50 km	B2
UCM(*)	a2	PROMES	HadAM3H	50 km	A2
UCM	b2	PROMES	HadAM3H	50 km	B2
DMI(*)	HS1	HIRHAM	HadAM3H	50 km	A2
DMI	HS2	HIRHAM	HadAM3H	50 km	A2
DMI	HB1	HIRHAM	HadAM3H	50 km	B2
DMI	S25	HIRHAMh	HadAM3H	25 km	A2
DMI	ecscA2	HIRHAM	ECHAM4	50 km	A2
DMI	ecscA2	HIRHAM	ECHAM4	50 km	B2
ETH(*)	HC-A2	CHRM	HadAM3H	55 km	A2
GKSS(*)	SA2	CLM	HadAM3H	55 km	A2
HC(*)	adhfa	HadRM3P	HadAM3H	50 km	A2
MPI(*)	3005	REMO	HadAM3H	55 km	A2
SMHI(*)	HCA2	RCAO	HadAM3H	50 km	A2
SMHI	HCB2	RCAO	HadAM3H	50 km	B2
SMHI	MPIA2	RCAO	ECHAM4	50 km	A2
SMHI	MPIB2	RCAO	ECHAM4	50 km	B2
SMHI	HCA222	RCAOh	HadAM3H	22 km	A2

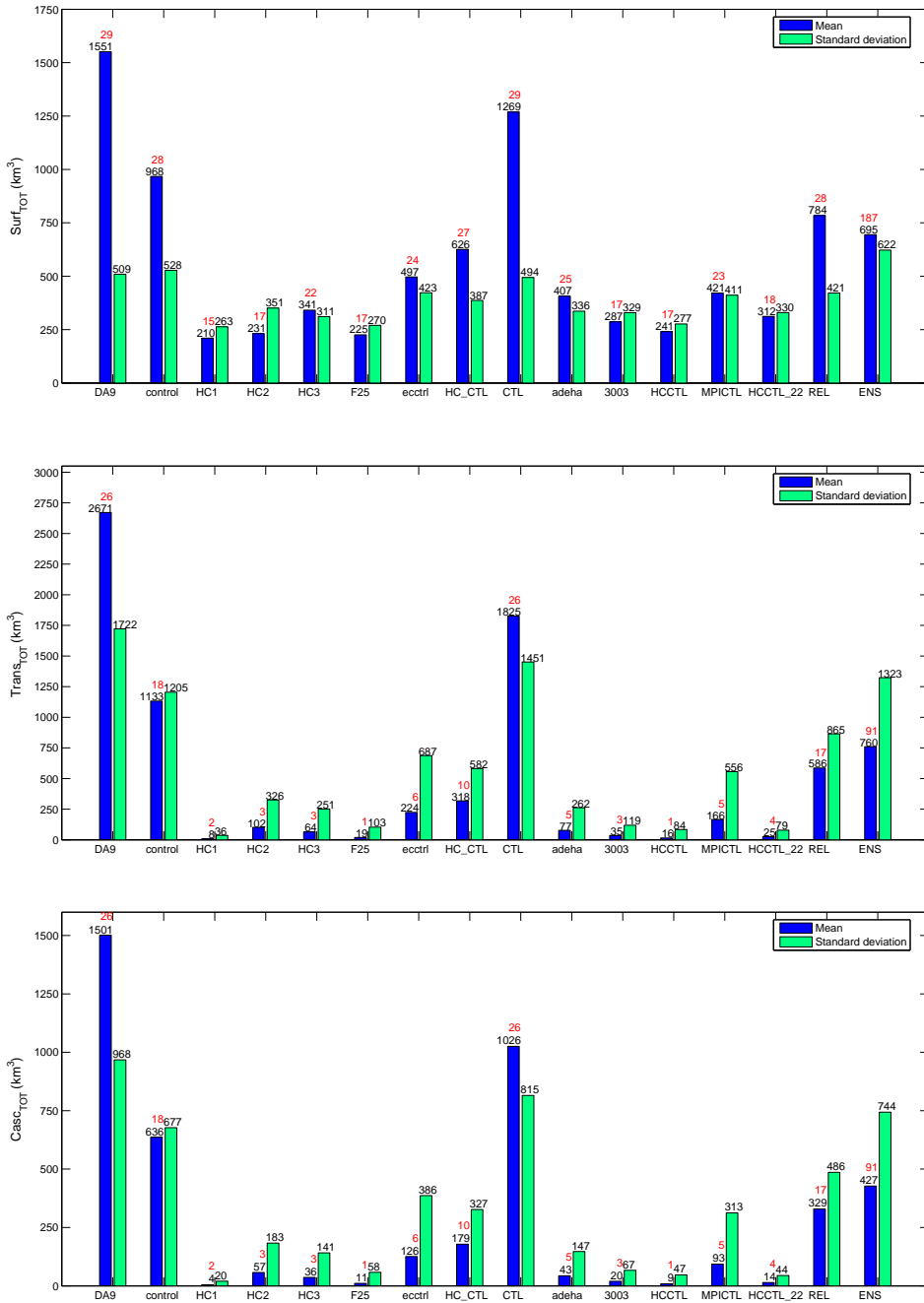


FIG. 9.12 – Average and standard deviation of the DW formed at the surface $Surf_{TOT}$, exported $Trans_{TOT}$, and cascading $Casc_{TOT}$ for each present-day climate simulation selected from the PRUDENCE project, for the REL set and for the mean ensemble ENS (km³).

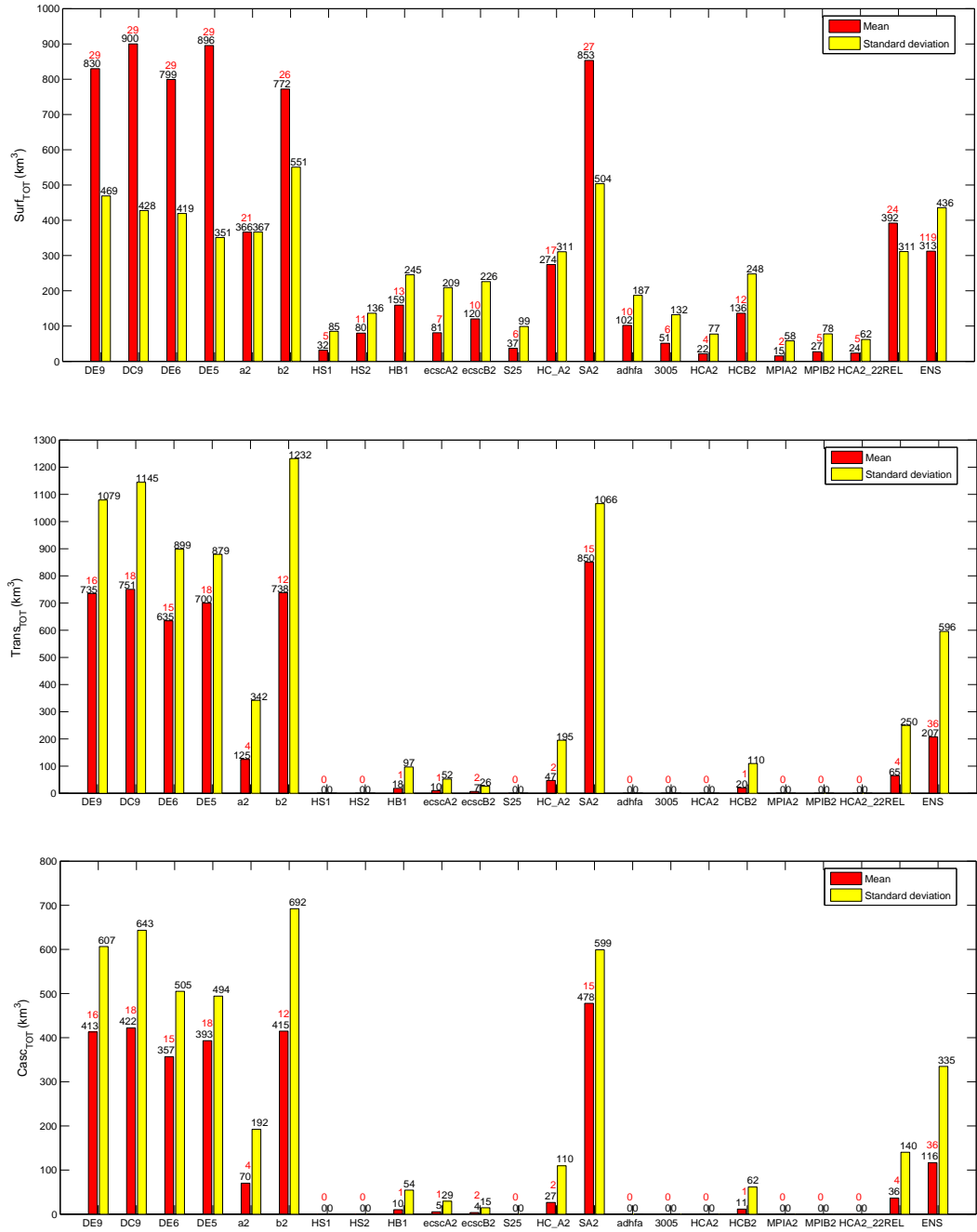


FIG. 9.13 – Average and standard deviation of the DW formed at the surface $Surf_{TOT}$, exported $Trans_{TOT}$, and cascading $Casc_{TOT}$ for each XXIth century simulation selected from the PRUDENCE project, for the REL set and for the mean ensemble ENS (km³).

by *Jacob et al.* [2007], one observes an important variability of the heat loss among the ARCMs, both for the present and future periods, with a 2.3 factor between the weaker and stronger heat losses.

The relationships established in Section 9.5 are used to estimate the quantities of DW formed at the surface, exported and cascading for each year of each simulation. The results for REL actually corresponds to results obtained in Section 9.5. The ORCM presented in Section 9.2.1 was not forced by all the different ARCMs compared here. The stratification is therefore assumed to be given by the simulation performed with the ORCM forced by ARPEGE-Climate : $HL_{strat,p}$ and $HL_{strat,f}$ computed in Section 9.4 are used for every simulations. The average and standard deviation of the resulting quantities for each simulation are presented on Fig. 9.12 and 9.13.

The different uncertainties are summarized and quantified in Table 8. To quantify the uncertainty due to the choice of the ARCM, we compute the standard deviation of the results obtained for the different runs of the ensemble mean. For the other uncertainties, we compute

$$\sqrt{\frac{\sum_{Institutes} \left[\sum_{runs} (value(Institute, run) - \overline{value(Institute)})^2 \right]}{\left(\sum_{Institutes} number\ of\ runs \right) - 1}} \quad \text{where } \overline{value(Institute)} \text{ is the average}$$

value obtained by an institute over different runs aimed at testing a given type of uncertainty.

Impact of the choice of the ARCM

The results show a strong sensitivity to the atmospheric ARCM, with two orders of magnitude between the most productive and least productive model in terms of DW (Fig. 9.12 and 9.13 and Table 8). For each run, and for both periods, the standard deviation is strong, of the same order as the average, showing that the strong interannual variability of the DW formation, export and cascading is reproduced by each model (Fig. 9.12 and 9.13). Considering that the ensemble mean was shown to perform better for the present period than the individual models [*Jacob et al.*, 2007], the results obtained for ENS provide an estimate of the mean annual surface formed ($690\ km^3$), exported ($760\ km^3$) and cascading ($430\ km^3$) DW volume under present-day climate conditions, with standard deviations of the same order, showing the high interannual variability of these processes. These results are close to the results obtained for REL, of respectively $788\ km^3$, $597\ km^3$ and $335\ km^3$, corresponding to differences of +14%, -21% and -22% with the results obtained for ENS. The cascading volume obtained for the ensemble mean is also in the range of the observational data mentionned in Section 9.3.

Table 7 presents the ratio of HL_{DJFM} , *Surf*, *Trans* and *Casc* for each simulation of the 2071-2100 period compared with the corresponding simulation of the 1961-1990 period. For the A2 scenario, the change of the heat loss varies between -17% (MPIA2) and +18% (HS2), and is very small (-2%) for the ensemble mean. For this scenario, the formation, export and cascading decrease for all the simulations, with decrease of cascading varying between 63% and 100 %. For the future period, the ensemble mean shows decreases of DW formation, export and cascading by of 65%, 74% and 73%. In Section 9.5, we obtained decreases of 50%, 90% and 89% for REL. Examining the distribution of the quantities obtained with the ensemble mean (Fig.

9.14), surface formation occurs 75% of the years, and export and cascading occurs 65% of the years in the present period. For the future period, these values decrease to 45% and 15%. As explained in Section 9.5, the fact that the mean export is higher than the mean surface formation under present-day climate (Fig. 9.14) is due to the years with the strongest heat losses. This happens also for some years of the future period, but only exceptionally, because of the stronger stratification.

Impact of the natural variability

Three ensemble simulations performed by the DMI using the same model but changing only the initial conditions were available for the present period (HC1, HC2 and HC3), and two for the future period (HS1, HS2). This enables to test the sensitivity of the model results to the climate variability. This does not have a very strong effect neither on the mean heat loss nor on its variability (see Fig. 9.11). The impact of the climate variability on the DW formed, exported and cascading in the present and future periods is negligible compared to the impact of the ARCM (Fig. 9.12 and 9.13 and Table 8).

Impact of the spatial resolution of the ARCM

The DMI and SMHI institutes used higher resolution models (HIRHAMh and RCAOh instead of HIRHAM and RCAO) to perform simulations for the present period (F25 and HCCTL22, to be compared with HC1,2,3 and HCCTL, see Table 5) and for the future period (S25, HCA222, to be compared with HS1,2 and HCA2, see Table 6). For both periods, the model resolution does not have a significant impact, neither on the heat loss nor on the DW quantities, compared to the impact of the ARCM (Fig. 9.12 and 9.13 and Table 8).

Impact of the choice of the AOGCM

Those two institutes also performed simulations with a different bounding AOGCMs (ECHAM4 instead of HadAM3H) for the present period (ecctrl and MPICTL) and for the future period (ecscA2 and MPIA2). For the present period, the impact on the DW quantities is more important than the impact of the resolution or the climate variability (Fig. 9.12 and Table 8) : for both models, the AOGCM change results in an increase of the surface formation by a factor of 2 (for the DMI, the ecctrl run is compared with the mean of the HC1, HC2 and HC3 runs), and of the export and cascading by a factor of 10 for SMHI and 3.5 for DMI. For the future period, this impact is negligible. For both models, the impact of the choice of the AOGCM on the decrease of surface formation, export and cascading is negligible compared to the impact of the ARCM (Table 8).

Impact of the choice of the scenario

The CNRM, UCM, DMI and SMHI institutes performed simulations changing only the scenario from A2 to B2 (DC9, DE5, b2, HB1, ecscB2, HCB2 and MPIB2, to be compared with DE9, DE6, a2, HS1, escA2, HCA2 and MPIA2). The impact of the scenario varies among the simulations (Table 7), and the uncertainty due to the scenario is half the uncertainty due to the choice of the ARCM (Table 8). For DC9,

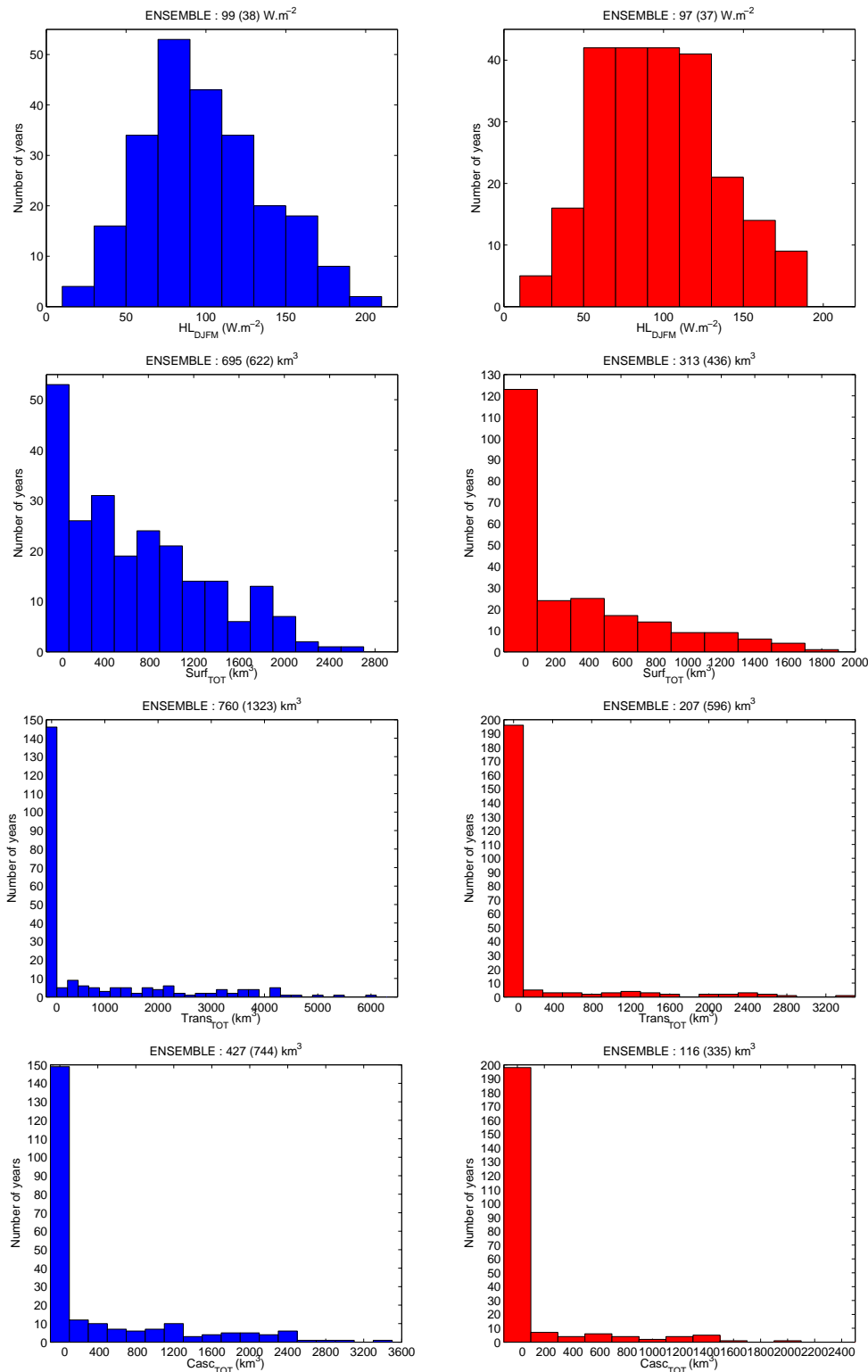


FIG. 9.14 – Distribution of the heat loss HL_{DJFM} ($\text{W} \cdot \text{m}^{-2}$) and of the DW formed at the surface $Surf_{TOT}$, exported $Trans_{TOT}$, and cascading $Casc_{TOT}$ for the mean ensemble ENS (km^3) under present-day climate conditions (left) and at the end of the XXIth century (right). The average and standard deviation are indicated.

DE5, and MPIB2, the decreases of the heat loss and of SW formation, export and cascading are comparable to the decrease obtained with the A2 scenario (DE9, DE6 and MPIA2). For ecscB2, the heat loss slightly increases (+6%) whereas it slightly decreases in escA2 (-7%) however, surface formation, export and cascading decreases are comparable. For the run b2 the heat loss increases by 15%, whereas it decreases by 8% for a2, and the surface formation, export and cascading decrease for b2 is half that for a2. For HB1 and HCB2, the heat loss increases by more than 30%, surface formation still decreases, but less than in the A2 simulations, and export and cascading even increase compared to the present period.

To summarize, the uncertainty in the modeling of DW formation, export and cascading is mostly due to the choice of the ARCM in the present and future periods and the scenarios in the future period. The model resolution, the choice of the forcing AOGCM and the natural variability of the climate have much weaker impacts, of at least one order of magnitude smaller (Table 8). The strong interannual variability of these processes is reproduced by every model. For the A2 scenario, DW formation, export and cascading decrease in all the simulations by at least 30%, 50% and 50%, and in average, using the ENS mean, cascading is reduced by more than 70% at the end of the 21st century. Globally, results obtained for ENS and for REL are quite similar, with a maximum difference of 20 %. Note that the uncertainty due to the vertical stratification is certainly important, but could not be assessed in the present study because of a lack of ORCM simulations due to the large numerical cost of such ORCM experiments : the ORCM used to force SYMPHONIE was only forced by one ARCM (see Section 9.2.1), and not by the other ARCMs compared in this section.

9.7 Conclusion

A regional oceanic circulation model was used in this study to examine the effects of interannual atmospheric variability and climate change on DW formation over, export from and cascading off the Gulf of Lions shelf. This model was forced at its lateral and surface boundaries by a 140-year basin-scale simulation performed over the whole Mediterranean Sea. Seven years were selected in the present and future periods.

The analysis of the simulations for the selected years of the present period enabled to study the impact of interannual variability. Volumes of DW formed, exported and cascading are strongly related to the average heat loss during the December-March period. The interannual variability is strong for the three quantities, of the same order as the average values. Surface formation occurs every year, however, export and cascading occurs only for years colder than the average. The characteristics of DW formation and export (volumes, current velocity, density contrast, spatial variability) are in agreement with the observations.

For the selected years of the future period, surface formation still occurs, but for an equivalent heat loss, formed volume is smaller than for the present period. There is only one year with non zero export and cascading, with volumes an order of magnitude smaller than volumes obtained for cold years of the present period. The decrease of DW formation and export is not due to a decrease of the winter heat

TAB. 9.7 – Ratios of the winter heat loss HL_{DJFM} , and the yearly surface formation rate $Surf$, export $Trans$ and cascading $Casc$ between the 2071-2100 simulations and the corresponding 1961-2100 simulation.

Run name	HL_{DJFM}	$Surf$	$Trans$	$Casc$	Sc.
DE9 / DA9	0.93	0.54	0.28	0.28	A2
DC9 / DA9	0.95	0.58	0.28	0.28	B2
DE6 / DA9	0.92	0.52	0.24	0.24	A2
DE5 / DA9	0.95	0.58	0.26	0.26	B2
a2 / control	0.92	0.38	0.11	0.11	A2
b2 / control	1.15	0.80	0.65	0.65	B2
HS1 / HC1	1.03	0.15	0.00	0.00	A2
HS2 / HC2	1.18	0.35	0.00	0.00	A2
HB1 / HC1	1.37	0.76	2.25	2.50	B2
S25 / F25	0.89	0.16	0.04	0.04	A2
ecscA2 / ecctrl	0.93	0.24	0.03	0.03	A2
ecscB2 / ecctrl	1.06	0.16	0.00	0.00	B2
HC-A2 / HC-CTL	1.05	0.44	0.15	0.15	A2
SA2 / CTL	1.05	0.67	0.47	0.47	A2
adhfa / adeha	0.92	0.25	0.00	0.00	A2
3005 / 3003	1.00	0.18	0.00	0.00	A2
HCA2 / HCCTL	0.96	0.09	0.00	0.00	A2
HCB2 / HCCTL	1.30	0.56	1.25	1.22	B2
MPIA2 / MPICTL	0.73	0.04	0.00	0.00	A2
MPIB2 / MPICTL	0.79	0.06	0.00	0.00	B2
HCA222 / HCCTL22	0.93	0.08	0.00	0.00	A2
REL / REL	1.15	0.50	0.11	0.11	A2
ENS /ENS	0.98	0.45	0.26	0.27	A2

TAB. 9.8 – Classification of the uncertainties. For the uncertainty due to the choice of the ARCM, standard deviation of the results obtained with the different runs of the ensemble mean. For the other uncertainties,

$$\sqrt{\frac{\sum_{Institutes} \left[\sum_{runs} (value(Institute, run) - \overline{value(Institute)})^2 \right]}{\left(\sum_{Institutes} number\ of\ runs \right) - 1}} \quad \text{with } \overline{value(Institute)} \text{ the average value}$$

obtained by an institute over different runs aimed at testing a given type of uncertainty. The values obtained for the ensemble mean are also indicated. Unit : km³

Uncertainty	<i>Surf</i>	<i>Trans</i>	<i>Casc</i>
Present period			
ARCM	512	1016	571
Natural variability	70	47	27
Resolution	30	6	4
AOGCM	138	107	60
Value(ENS)	695	760	427
Future period			
ARCM	340	338	190
Natural variability	34	0	0
Resolution	2	0	0
AOGCM	20	4	2
Scenario	132	178	100
Value(ENS)	313	207	116

loss, which actually slightly increases between the present and future periods, but to the stronger stratification induced by the decrease of the annual buoyancy loss during the 21st century.

Results obtained for the selected years are extrapolated to the whole 30-year present and future periods using linear regression for the surface formation and non-linear regression for the export and cascading. This statistic method enabled to establish a relationship between the volumes and the difference between the winter atmospheric heat loss and the heat loss necessary to increase the shelf water density up to the DW criteria. This latest heat loss is stronger in the future period compared to the present period ($\sim +30 \text{ W.m}^{-2}$), because of the stronger stratification. For the present period, values of $\sim 800 \text{ km}^3$, $\sim 600 \text{ km}^3$ and $\sim 300 \text{ km}^3$ are obtained for the 30-year average volume of water formed, exported and cascading. These values are reduced by respectively 50%, 90% and 90% by the end of the 21st century.

Under the assumptions used in the present study, DW cascading practically disappears by the end of the 21st century. Such a change would have a tremendous impact on the deep ecosystems functioning, highly dependent on the quantity of nutrients provided by the DW coming from the shelf, and on the local carbon storage into the deep ocean.

Sensitivity tests to the choice of the DW density criteria, the parameters of the regional oceanic model, the water flux, the atmospheric forcing model and the scenario were performed. The uncertainty related to the forcing ARCM is the strongest, with two orders of magnitude between the most and least productive models in terms of DW, due to the high variability of the winter heat loss among the models. Nevertheless, the relative change between the present-day climate conditions and the 21st century does not change a lot among the forcing ARCMs. The scenario has also a strong impact, with differences between A2 and B2 scenarios varying a lot among the models.

Due to technical constraints, it was not possible to perform a 140-year simulation with the regional oceanic model. However, the time-computing costs are weaker and weaker due to technological advances, and it should be possible in the near future to perform 30 one-year simulations for the present period and for the future period. This method would give more precise information about the interannual variability and would enable to quantify more accurately the average annual rates.

It would also be very interesting to force the basin-scale ORCM using different ARCMs and scenarios to evaluate the impact of the stratification on our results. Such simulations should be available in the future thanks to the CIRCE project (<http://www.bo.ingv.it/circeip/>). In the present study, due to a lack of ORCM simulations, the stratification was indeed considered independent on the ARCM. However, one can expect a rather "cold" or "warm" ARCM to produce different stratifications. This could be even more important for the future : the change of stratification induced by the evolution of the atmosphere during the 21st century would most certainly change depending on the ARCM and on the scenario. Note however that other climate change studies performed over the Mediterranean Sea [Thorpe and Bigg, 2000; Bozec, 2006] also predicted a weakening of the Mediterranean thermohaline circulation and a decrease of the surface density by the end of the 21st century, and therefore an increase of the stratification.

In this paper, we propose a downscaling strategy to investigate the regional impacts of short and long terms climate variability, going from global climate models to a

basin ocean circulation model and finally to a high-resolution model. The enhancement of the stratification induced by climate change appears to have a considerable impact on the particular process studied here, i.e. the formation and fate of dense water on the continental shelf. We focused our study on the Gulf of Lions, but this methodology could be used to study the effects of climate variability in other regions where cascading occurs [Ivanov *et al.*, 2004; Durrieu de Madron *et al.*, 2005]. In particular, DW cascading occurring in the Adriatic and the Aegean seas could also be strongly affected by the increase of the stratification in the Mediterranean sea. At a more global scale, the decrease of the stratification induced by the slowing of the Atlantic meridional overturning observed by Bryden *et al.* [2005] could affect the huge quantities of DW cascading in the North Atlantic and Arctic continental shelves. Finally, this downscaling approach could be applied to examine the regional impact of climate change on other regional circulation processes (wind induced circulation, mesoscale processes ...).

Acknowledgments

Data have been provided through the PRUDENCE data archive (*prudence.dmi.dk*), funded by the EU through contract EVK2-CT2001-00132.

